

pubs.acs.org/JPCL Letter

Effect of Extreme Variations of Fundamental Constants on the Structure of Atoms and Molecules

Vsevolod D. Dergachev, Hoang Bao Tran Tan, Sergey A. Varganov,* and Andrei Derevianko*



Cite This: J. Phys. Chem. Lett. 2024, 15, 4111-4116



Read Online

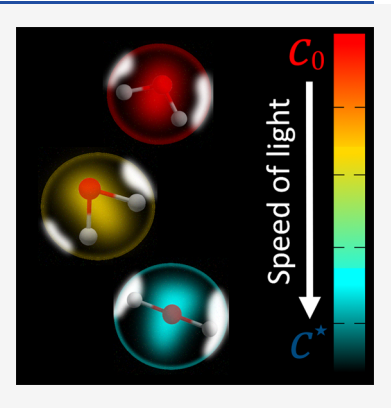
ACCESS I

III Metrics & More

Article Recommendations

s Supporting Information

ABSTRACT: The fundamental constants (FCs) of physics are promoted to dynamic quantities in modern theories. Heretofore, astrophysical observations, atomic clock experiments, and the Oklo natural nuclear reactor phenomenon all have pointed to small variations of FCs happening on a cosmologically long time scale. In this paper, we investigate the novel regime of extreme but transient variations of FCs. We focus on the speed of light (c) and show that its variation can dramatically change the electronic structure and chemistry of atoms and molecules. These changes are induced by increased relativistic effects when c is reduced from its nominal value. To model these changes, we solve the fully relativistic Dirac equation at different values of c. We show that at extreme variations of c, the periodic table is truncated, the nominal ground states of atoms can change, water fails to serve as a universal solvent, and the ammonia molecule becomes planar.



uantum chemistry primarily depends on a set of three fundamental constants (FCs): electron mass m_e , elementary charge e, and Planck constant \hbar . Relativity brings in speed light c or, equivalently, fine-structure constant $\alpha = e^2/(\hbar c)$. These constants, together with the nuclear parameters, are fixed in conventional computations to their empirical (nominal) values. Modern theories, however, generically promote these FCs to dynamic entities, $^{1,2}_{-}$ and their small variations have been previously studied. In this paper, we explore a novel regime of extreme but transient variations that are motivated by certain clumpy dark matter models. We find that strong variations of c afford an abundance of remarkable effects on the structure of atoms and molecules and, by extension, on the fundamental conditions for the emergence and sustainability of life, i.e., the so-called anthropic principle in cosmology. 10,11

The variation of FCs in the nonrelativistic Born–Oppenheimer (NR-BO) approximation reduces to the isotropic scaling of all nuclear and electronic coordinates by the Bohr radius $a=\hbar^2/m_e e^2$ (see Section I of the Supporting Information). As a result, molecular bond angles do not depend on the FCs. Similarly, all of the FC dependence of energies factorizes out via the Hartree energy, $m_e e^4/\hbar^2$. Effects beyond the NR-BO approximation violate these scaling laws and lead to changes in the bond angles with varying FCs. For the sake of concreteness, we focus on the role of relativity and examine the consequence of varying speed of light c. In atomic units, $\alpha=1/c$, and variations in α are equivalent to those in c via $c/c_0=\alpha_0/\alpha$. Here and below, the subscript 0 of a quantity refers to its nominal value, e.g., $\alpha_0\approx 1/137$.

Beyond connections to novel theories, there is a practical utility in artificially enhancing relativity. 12 Because an electron

near the nucleus of charge Z moves with speed $v/c \sim \alpha Z$, relativistic effects are most pronounced in heavy systems. However, in heavy atoms and molecules, the role of relativity is often masked by large electron correlations. Reducing c magnifies the role of relativity in molecules comprising light atoms, where correlations can be treated with much higher accuracy. ^{13–15} It is worth emphasizing that for small speeds of light, $v/c \sim 1$, and one must solve the nonperturbative four-component Dirac equation. ^{16,17} We find that when $c \sim c_0/10$ to $c_0/20$, the periodic table shrinks to elements from hydrogen to sulfur, the Aufbau principle qualitatively changes, noble gases are no longer inert, water fails to serve as a universal solvent, and the ammonia molecule becomes planar.

We start by discussing the effect of the varying speed of light on the electronic structure of a hydrogen-like atom. In atomic units, its ground state energy can be obtained by solving the Dirac equation with a point-like nucleus approximation

$$\varepsilon_{1s_{1/2}} = c^2 \left[\sqrt{1 - (Z/c)^2 - 1} \right]$$
 (1)

The Dirac equation has two continua: above the ionization threshold, $\varepsilon > 0$, and below the rest-mass gap, $\varepsilon < -2c^2$. In the Dirac sea paradigm, ¹⁸ the lower continuum is fully occupied by electrons so an atomic electron cannot spontaneously decay

Received: February 24, 2024 Revised: March 26, 2024 Accepted: March 28, 2024



into the lower continuum because of the Pauli exclusion principle. As we decrease c, the $1s_{1/2}$ energy in eq 1 is decreased toward the Dirac sea until we reach a value of c=Z whereupon $\varepsilon_{1s_{1/2}}=-c^2$. When c<Z, the argument of the square root, $1-(Z/c)^2$, becomes negative and the energy acquires an imaginary part; the ground state of a hydrogen-like atom becomes unstable.

The point-like nucleus approximation in eq 1 is, however, inadequate for determining the critical value of c. This is because the bound states become unstable when their energies "dive" into the Dirac sea, 19,20 i.e., at $\varepsilon_{1s_{1/2}} = -2c^2$, and not at $-c^2$ as per eq 1. To remedy the failure of the point-like nucleus approximation, one solves the Dirac equation with finite-size nuclei numerically (Figure 1a). As expected, the hydrogen

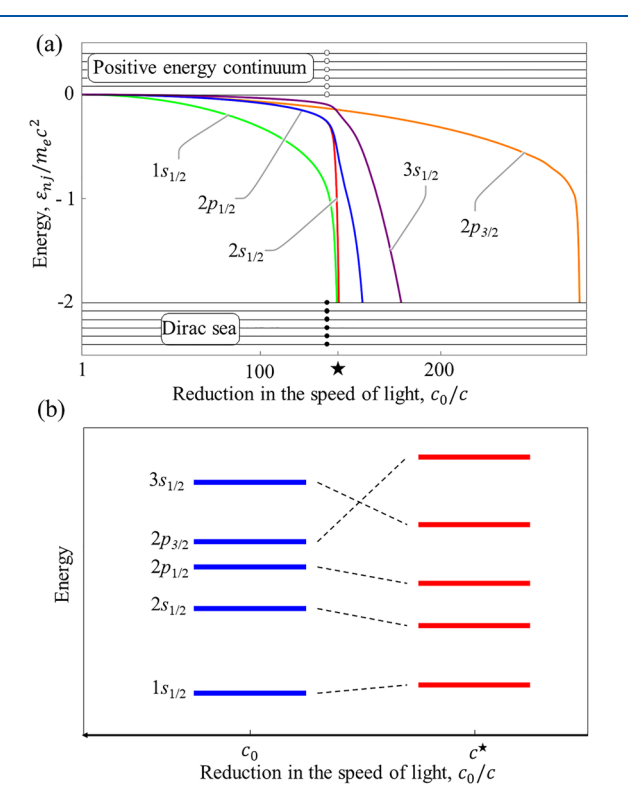


Figure 1. Dependence of the atomic energy levels of a hydrogen-like atom on speed of light c. (a) Energy levels of atomic hydrogen as a function of c. The $1s_{1/2}$ level dives into the Dirac sea at $c^* \approx c_0/143$. (b) Change in shell occupation in many-electron atoms with varying c.

atom remains stable until its ground state energy dives into the Dirac sea. The $1s_{1/2}$ energy breaches the rest-mass energy gap at the critical value of $c^* \approx c_0/143$. The question of what happens when c is driven below its critical value c^* has been explored in a related problem of determining the critical nuclear charge with c fixed to its nominal value. When $c < c^*$, the discrete $1s_{1/2}$ level becomes embedded into the Dirac sea continuum and, as such, becomes unstable, similar to Fano resonances in chemical physics. An electron—positron pair is emitted spontaneously, and the vacuum becomes electrically charged. The critical value c^* at which the 1s level in an atom with charge Z becomes unstable changes with the nuclear charge as (see Section II of the Supporting Information)

$$\frac{c^{\star}}{c_0} = \frac{\alpha_0}{\alpha^{\star}} \approx \frac{Z}{168} \tag{2}$$

This remains a good approximation for multielectron systems as the $1s_{1/2}$ electrons tend to see the unscreened nuclear charge with minor correlation corrections to binding energies. In a molecule, c^* is determined by the charge of the heaviest nucleus. For water and ammonia discussed below, $c^* \approx c_0/18.4$ and $c^* \approx c_0/20.9$ are determined by the oxygen and nitrogen atoms, respectively. From eq 2, we observe that at a given value of c/c_0 , only elements for which $Z \lesssim 168c/c_0$ are stable. As c is gradually decreased from its nominal value, the heavier elements are destabilized and the periodic system is truncated. If c is reduced 10-fold, only elements for which $C \lesssim 16$ remain stable, and the entire periodic table shrinks to elements from hydrogen to sulfur. If c is reduced to that of a speeding bicycle, $c/c_0 \approx 4 \times 10^{-8}$, even the hydrogen atom fails to exist.

Let us next discuss atomic levels above the 1s electron shell. The Aufbau principle determines the sequence of how atomic orbitals are filled with electrons. In the spin—orbital notation, the sequence is $1s_{1/2}2s_{1/2}2p_{1/2}2p_{3/2}3s_{1/2}$ at $c\approx c_0$. In the ultrarelativistic regime, when c approaches its critical value, we find that the $2p_{3/2}$ and $3s_{1/2}$ orbitals change their relative energy order (Figure 1b). Figure 2 shows the implication of

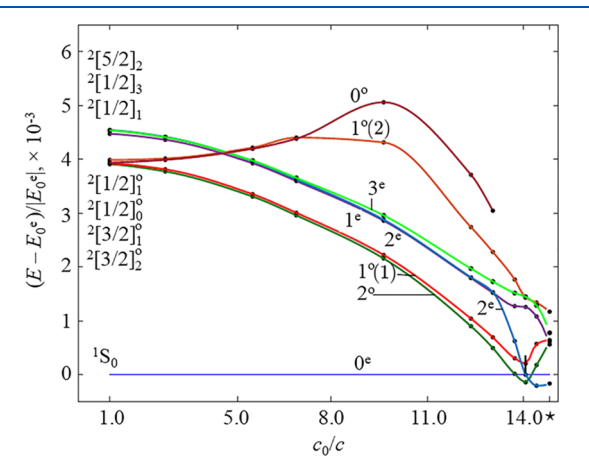


Figure 2. Energy spectrum of the neon atom as a function of the speed of light $(c_0/c = \alpha/\alpha_0)$. Nominal ground state $0^{\rm e}$ ($^1{\rm S}_0$) is used as a reference (blue horizontal line). There is a substantial reshuffling of the sequence of energies near the critical value of $c^{\star} \approx c_0/14.8$. The ground state of the neon atom becomes the $2^{\rm e}$ state with the dominant open-shell configuration $1s_{1/2}^2 2s_{1/2}^2 2p_{1/2}^2 3s_{1/2}^2 2p_{3/2}^2$.

the change in the relative energy order between $2p_{3/2}$ and $3s_{1/2}$ on the energy spectrum of the neon atom. At nominal values of c, the states are labeled using the conventional L—S coupling scheme. 23,24 At smaller values of c, the states are labeled as J^{π} , where J is the total angular momentum and π is the parity of a state. When $c \lesssim c^{\bigstar} \approx c_0/14$, the ground state of neon contains the configuration $1s_{1/2}^2 2s_{1/2}^2 2p_{1/2}^2 3s_{1/2}^2 2p_{3/2}^2$ with the total angular momentum J=2. Thus, neon becomes an openshell atom with the $2p_{3/2}$ shell only half-filled and, as such, is no longer inert. The valence-shell configuration of the ultrarelativistic neon, $3s_{1/2}^2 2p_{3/2}^2$, closely resembles that of carbon at nominal c, $2s^22p^2$. Therefore, at such an extreme transient variation of c, neon is expected to play the traditional role of carbon.

Our calculations for the second-period atoms with electrons in the $2p_{3/2}$ shell (N, O, F, and Ne) demonstrate similar

nontrivial changes in the nature of their ground states near their respective critical c (see Section III of the Supporting Information). Qualitatively, the $2p_{3/2}$ orbital dives into the Dirac sea at a c substantially smaller than that for $2p_{1/2}$ (Figure 1a). This leads to a giant $\sim m_c c^2$ fine-structure splitting near the critical value c^{\star} . For the same reason, there is a large difference in the relativistic contraction of the $2p_{3/2}$ and $2p_{1/2}$ shells near c^{\star} . The $2p_{1/2}$ and $3s_{1/2}$ shells become submerged inside the $2p_{3/2}$ shell. This drives a more effective screening of the nuclear charge by the inner shells, causing an increase in the $2p_{3/2}$ orbital energies with a decrease in c in many-electron atoms, a trend that is the opposite of that in the H-like ions. These effects also lead to dramatic changes in the geometry of molecules containing these atoms.

Let us now discuss how extreme variation of the speed of light affects the structure and properties of molecules. As examples, we focus on water and ammonia. All known forms of life use water as a universal solvent for various chemicals and as an essential component of many metabolic processes. Ammonia is an important source of nitrogen required for the synthesis of amino acids, for building proteins in living systems, and as an alternative universal solvent. The structural changes induced by the enhanced relativity in these molecules can be explained by changes in their respective molecular orbitals (MOs). The formation of MOs requires energy resonances and overlaps among the constituent atomic orbitals. Relativity affects the resonances via the different rates of stabilization of energies and the overlaps via the varying degrees of contraction of atomic orbitals.

When the speed of light is reduced, the geometry of the water molecule changes with the initial contraction of the bond angle and the subsequent complete straightening of the molecule (Figure 3a–c). We find that when $c \approx c_0/14$, the calculated bond angle in water decreases from the nominal value of 104.5° to 90°. This corresponds to the dipole moment of water μ increasing from its nominal value of 1.855 D²⁷ to 2.138 D. When $c \approx c_0/18$, the water molecule becomes linear and therefore nonpolar ($\mu = 0$ D). These changes in the molecular geometry are induced by the relativistic stabilization of the $2s_{1/2}$ and $3s_{1/2}$ orbitals with respect to the 2p orbitals of the oxygen atom, and by increased fine-structure splitting between the $2p_{1/2}$ and $2p_{3/2}$ orbitals. These changes can be understood using the valence-shell electron-pair repulsion (VSEPR) and MO models.²⁸

- (i) At nominal $c=c_0$, the valence 2s and 2p atomic orbitals of oxygen mix to form four equivalent sp³ $(2s_{1/2}2p_{1/2}2p_{3/2})$ hybridized orbitals. Two of the hybrid orbitals overlap with the hydrogen 1s orbitals, and the remaining two hold two lone electron pairs. The repulsion between the four electron pairs on the hybrid orbitals leads to the slightly distorted tetrahedral arrangement, corresponding to a bond angle of 104.5° .
- (ii) At the intermediate $c \approx c_0/14$, the stabilization of the $2s_{1/2}$ and $2p_{1/2}$ orbitals in oxygen breaks down the sp³ hybridization. This results in an energetically isolated $2p_{3/2}$ orbital, which can accommodate up to four electrons forming the oxygen—hydrogen bonds. This stabilizes the molecular structure, resulting in a 90° bond angle. The stabilization of the $2s_{1/2}$ and $2p_{1/2}$ atomic orbitals also changes the distributions of the electron radial density in water (see Section IV of the Supporting Information). The computed radial density distributions of HOMO—2 and HOMO—3 reduce to those of $2s_{1/2}$ and $2p_{1/2}$ atomic orbitals, which no longer participate in chemical bonding.

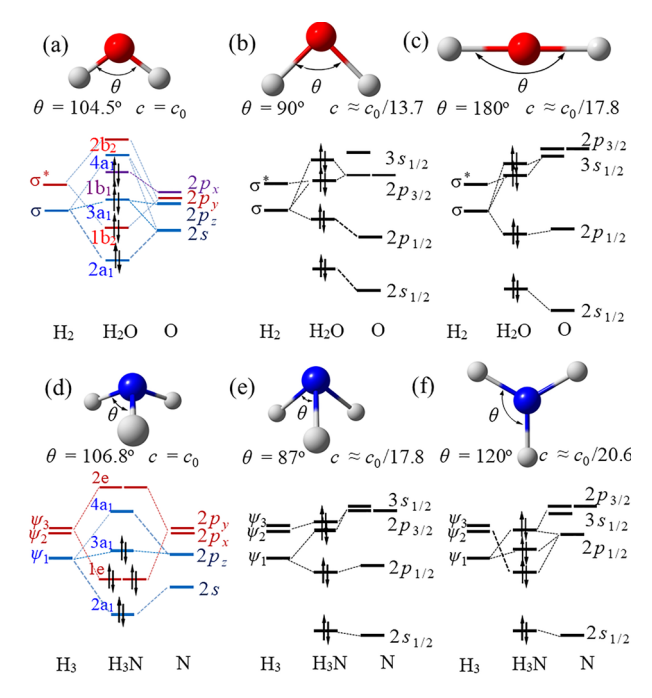


Figure 3. Molecular geometries and orbital diagrams of (a and c) water and (d and f) ammonia calculated at different values of the speed of light. At a nominal c, the orbitals are labeled and colored according to their irreducible representations in the $C_{2\nu}$ (water) and $C_{3\nu}$ (ammonia) point groups. When $c < c_0$, the spin—orbital notation is used for atomic orbitals, and only the occupied molecular orbitals are shown.

(iii) At even smaller $c \approx c_0/18$, lowering the $3s_{1/2}$ and raising the $2p_{3/2}$ orbitals of oxygen lead to these two orbitals becoming quasi-degenerate. This induces the ps hybridization between the half-filled $2p_{3/2}$ and $3s_{1/2}$ shells, resulting in the linear molecular geometry. The participation of the $3s_{1/2}$ orbital in the chemical bonding is supported by our calculated radial density distribution for the HOMO-1 of water. Near c^* , the shape of this distribution closely resembles that of the $3s_{1/2}$ atomic orbital (see Section IV of the Supporting Information).

The Walsh correlation diagrams of the MO theory provide more insight into the relation between the electronic structure and the geometry of the water molecule (Figure 4a-c). These diagrams show the energies of valence MOs as a function of the bond angle. Because the total electron energy of a molecule can be approximated as the sum of MO energies, the Walsh diagrams can be used to predict the values of the bond angle that minimize the total energy. When $c=c_0$, the interplay between the HOMO-1 and HOMO-2 energies minimizes the total electron energy at a bond angle of 104.5° . As c decreases, the $2s_{1/2}$ orbital stabilizes and its contribution to HOMO is diminished, leading to the minimum of both HOMO and total energies at 90° . At an even lower speed of light, the realistically stabilized $3s_{1/2}$ orbital starts to contribute to the HOMO, leading to the linear geometry.

The changes in the molecular geometry of ammonia at a reduced speed of light resemble those of water and can be explained by the similarity of the changes in the electronic structures of the nitrogen and oxygen atoms. At the nominal speed of light, the VSEPR model predicts formation of four equivalent sp³ hybrid orbitals in nitrogen. Three of these orbitals form chemical bonds with the hydrogen atoms, while the fourth orbital holds the lone electron pair, leading to the

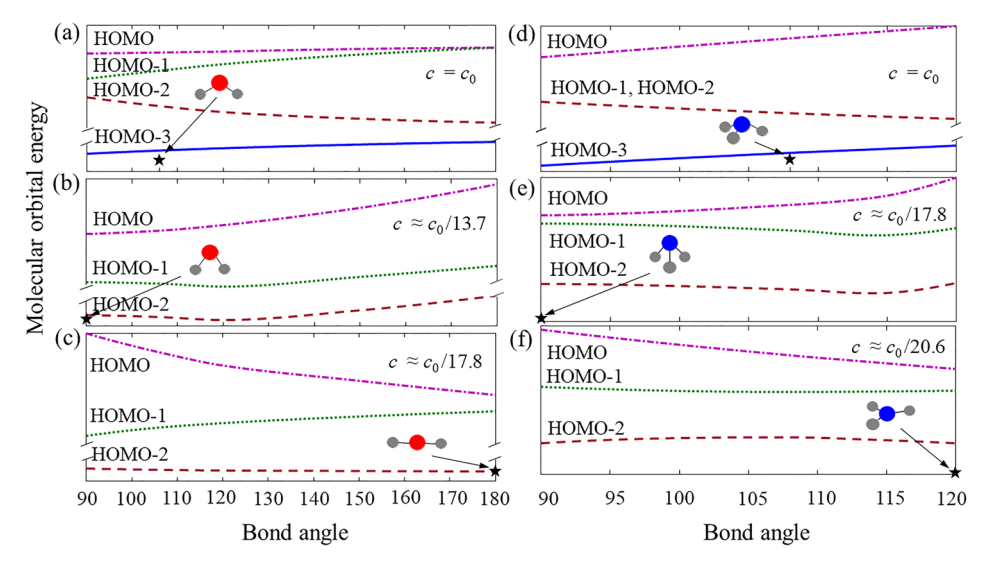


Figure 4. Walsh correlation diagrams of (a-c) water and (d-f) ammonia showing the energies of their respective valence MOs as a function of the bond angle at different speeds of light. For water, the orbital energies are calculated at (a) $c = c_0$, (b) $c \approx c_0/13.7$, and (c) $c \approx c_0/17.8$. For ammonia, the energies are calculated as (d) $c = c_0$, (e) $c \approx c_0/17.8$, and (f) $c \approx c_0/20.6$. In panels b, c, e, and f, which correspond to $c < c_0/10$, the lowest occupied MO of water (ammonia) is omitted as it reduces to the $2s_{1/2}$ atomic orbital of oxygen (nitrogen) and does not participate in the chemical bonding. The arrows indicate the bond angles at which the molecular geometries stabilize. The energies of the MOs at the equilibrium bond angles correspond to those in Figure 3.

trigonal pyramidal geometry with a bond angle of 106.8° (Figure 3d). As c decreases, the NH₃ molecule first becomes more pyramidal and subsequently flattens at values of c close to that of c^{\star} . When $c \approx c_0/18$, the bond angle in ammonia decreases to its minimum value of 87° (Figure 3e). This can be explained by the break of the sp³ hybridization due to the relativistic stabilization of the $2s_{1/2}$ atomic orbital of nitrogen. The reduction of the bond angle results in an increase in the dipole moment of ammonia μ from its nominal value of 1.561 D²⁹ to 2.028 D. An \sim 20-fold decrease in the speed of light leads to the planar geometry with a 120° bond angle (Figure 3f) and $\mu = 0$ D due to the induced quasi-degeneracy between the $2p_{3/2}$ and $3s_{1/2}$ orbitals. These observations are further supported by the calculated radial density distributions of the occupied MOs in ammonia (see Section IV of the Supporting Information).

The striking changes in the geometries of the oxygen- and nitrogen-containing molecules at reduced speeds of light would lead to alternative chemistry and biology. For example, in contrast to the bent water molecules that form threedimensional networks of hydrogen bonds, the ultrarelativisitc linear water molecules could form only two-dimensional networks. This is anticipated to substantially decrease the freezing and boiling points of water. 30,31 In addition, the linear water molecule would have no dipole moment. Thereby, water would cease to serve as a universal solvent. Clearly, life as we know it can happen only in a certain range of values of fundamental constants (the anthropic principle). 10,11 However, the current anthropic principle constraints on the slow cosmological-scale variation of FCs can be evaded for certain clumpy dark matter models that lead to transient variations. In these models, the FCs inside and outside of the dark matter clumps can differ substantially. Encounters of the solar system with dark matter clumps can be exceedingly rare, while the laboratory searches for possible encounters with such clumps so far extend over only a cosmologically short 20-year recent history.³² Our predicted changes in the geometry of ammonia, one of the most abundant polyatomic molecules in the

interstellar space,³³ can be potentially used in astrophysical searches for the dark matter clumps. As a clump sweeps through an interstellar cloud, for example, it would induce observable changes in the properties of the molecules comprising the cloud.

■ THEORETICAL METHODS

The critical values of the speed of light for the hydrogen atom and hydrogen-like ions were calculated by solving the Dirac equation with the finite nucleus models by using both analytical and numerical methods. The analytical c^* values were obtained from solving the transcendental eq S18 for α^* $1/c^*$ under the condition $\varepsilon = -2m_ec^2$ (the Dirac sea threshold) and using the nuclear spherical shell-like charge density distribution (see Section II of the Supporting Information). The numerical c^* values were obtained by solving the fourcomponent Dirac equation using the Dirac-Hartee-Fock (DHF) method³⁴ in DIRAC19.³⁵ The electronic state energies of N, O, F, and Ne were obtained by using the Kramer restricted configuration interaction (KRCI) method. The reference wave functions for the KRCI calculations were obtained by solving the average-of-configuration open-shell version of the DHF equation. In the averaging, all configurations generated by distributing the valence electrons over the 2s, 2p, and 3s orbitals were included. To accurately describe the electron density near nuclei and to ensure a balanced representation of the s and p orbitals needed for accurate prediction of the state energies at reduced c, the original uncontracted aug-cc-pV6Z basis set^{36,37} was modified as follows. We started with 11 s and 11 p functions using the p exponents of the original basis set for both types of functions. Then, the basis was augmented by one s and one p function with the exponents obtained by multiplying the current largest exponent by a factor of 3.0. The new basis was used to calculate the critical c for one-electron ions. New pairs of s and p functions were added until the calculated critical c matched the solution of the transcendental eq S18. The final basis

included 19 s and p functions. The number of the higherangular momentum functions and their exponents were unchanged. The molecular geometries of water and ammonia were optimized at different values of c using the closed-shell DHF method with the same augmented basis sets (see Section IV of the Supporting Information). Neglecting the effects of electron correlation in molecular calculations resulted in the deviation of the water and ammonia bond angles from their experimental values by <2%, which is sufficiently accurate for the purpose of this work. The dipole moments of water and ammonia were calculated at three selected geometries corresponding to the nominal, intermediate, and near critical values of c listed in the legend of Figure 4 by solving the nonrelativistic Schrödinger equation with scalar relativistic correction (see Section V of the Supporting Information). This approach is well justified because dipole moment mostly depends on molecular geometry, i.e., on the length of polar bonds and the bond angles, and therefore, the geometry changes induced by the reduction of the speed of light make the main contribution to the magnitude of the dipole moment.

ASSOCIATED CONTENT

5 Supporting Information

The Supporting Information is available free of charge at https://pubs.acs.org/doi/10.1021/acs.jpclett.4c00599.

Discussion of the invariance of molecular geometry under variation of fundamental constants in the nonrelativistic Born—Oppenheimer approximation, details of the calculation of the critical values of the speed of light in atoms, discussion of changes in the electronic structure of the N, O, F, and Ne atoms with varying speeds of light, and details of the electronic-structure calculations for molecules at different values of the speed of light (PDF)

Transparent Peer Review report available (PDF)

AUTHOR INFORMATION

Corresponding Authors

Sergey A. Varganov — Department of Chemistry, University of Nevada, Reno, Reno, Nevada 89557-0216, United States; orcid.org/0000-0001-8301-3891; Email: svarganov@unr.edu

Andrei Derevianko — Department of Physics, University of Nevada, Reno, Reno, Nevada 89557-0216, United States; Email: andrei@unr.edu

Authors

Vsevolod D. Dergachev – Department of Chemistry, University of Nevada, Reno, Reno, Nevada 89557-0216, United States

Hoang Bao Tran Tan — Department of Physics, University of Nevada, Reno, Reno, Nevada 89557-0216, United States; Los Alamos National Laboratory, Los Alamos, New Mexico 87545, United States

Complete contact information is available at: https://pubs.acs.org/10.1021/acs.jpclett.4c00599

Notes

The authors declare no competing financial interest.

ACKNOWLEDGMENTS

The authors thank X. Chu, M. Kozlov, A. Kusenko, and M. Pospelov for useful discussions. This work was supported by National Science Foundation Grants PHY-1912465, PHY-2207546, and CHE-1654547 and the Center for Fundamental Physics at Northwestern University.

REFERENCES

- (1) Uzan, J. P. Varying Constants, Gravitation and Cosmology. Living Reviews in Relativity 2011, 14, 2.
- (2) Safronova, M. S.; Budker, D.; DeMille, D.; Jackson Kimball, D. F.; Derevianko, A.; Clark, C. W. Search for New Physics with Atoms and Molecules. *Rev. Mod. Phys.* **2018**, *90*, No. 025008.
- (3) Dzuba, V. A.; Flambaum, V. V.; Webb, J. K. Space-Time Variation of Physical Constants and Relativistic Corrections in Atoms. *Phys. Rev. Lett.* **1999**, 82, 888.
- (4) Dzuba, V. A.; Flambaum, V. V.; Webb, J. K. Calculations of the Relativistic Effects in Many-Electron Atoms and Space-Time Variation of Fundamental Constants. *Phys. Rev. A* **1999**, *59*, 230.
- (5) Flambaum, V. V.; Dzuba, V. A. Search for Variation of the Fundamental Constants in Atomic, Molecular, and Nuclear Spectra. *Can. J. Phys.* **2009**, *87*, 25–33.
- (6) Webb, J. K.; King, J. A.; Murphy, M. T.; Flambaum, V. V.; Carswell, R. F.; Bainbridge, M. B. Indications of a Spatial Variation of the Fine Structure Constant. *Phys. Rev. Lett.* **2011**, *107*, No. 191101.
- (7) Windberger, A.; Crespo López-Urrutia, J. R.; Bekker, H.; Oreshkina, N. S.; Berengut, J. C.; Bock, V.; Borschevsky, A.; Dzuba, V. A.; Eliav, E.; Harman, Z.; et al. Identification of the Predicted 5s 4f Level Crossing Optical Lines with Applications to Metrology and Searches for the Variation of Fundamental Constants. *Phys. Rev. Lett.* **2015**, *114*, No. 150801.
- (8) Pašteka, L. F.; Hao, Y.; Borschevsky, A.; Flambaum, V. V.; Schwerdtfeger, P. Material Size Dependence on Fundamental Constants. *Phys. Rev. Lett.* **2019**, *122*, No. 160801.
- (9) Derevianko, A.; Pospelov, M. Hunting for Topological Dark Matter with Atomic Clocks. *Nat. Phys.* **2014**, *10*, 933–936.
- (10) Carter, B. Large Number Coincidences and the Anthropic Principle in Cosmology. *Proceedings of the International Astronomical Union* **1974**, *63*, 291–298.
- (11) Carr, B. J.; Rees, M. J. The Anthropic Principle and the Structure of the Physical World. *Nature* **1979**, 278, 605–612.
- (12) Dubillard, S.; Rota, J. B.; Saue, T.; Faegri, K. Bonding Analysis Using Localized Relativistic Orbitals: Water, the Ultrarelativistic Case and the Heavy Homologues H_2X (X=Te, Po, Eka-Po). J. Chem. Phys. **2006**, 124, No. 154307.
- (13) Sato, T. K.; Asai, M.; Borschevsky, A.; Stora, T.; Sato, N.; Kaneya, Y.; Tsukada, K.; Düllmann, C. E.; Eberhardt, K.; Eliav, E.; et al. Measurement of the First Ionization Potential of Lawrencium, Element 103. *Nature* **2015**, *520*, 209–211.
- (14) Kahl, E. V.; Raeder, S.; Eliav, E.; Borschevsky, A.; Berengut, J. C. Ab Initio Calculations of the Spectrum of Lawrencium. *Phys. Rev. A* **2021**, *104*, No. 052810.
- (15) Guo, Y.; Borschevsky, A.; Eliav, E.; Pašteka, L. F. Relativistic Coupled Cluster Calculations of the Electron Affinity and Ionization Potential of Nh (113). *J. Phys. B: At. Mol. Opt. Phys.* **2022**, *55*, No. 155003.
- (16) Dyall, K. G.; Fægri, K. J. Introduction to Relativistic Quantum Chemistry; Oxford University Press, 2007.
- (17) Reiher, M.; Wolf, A. Relativistic Quantum Chemistry. The Fundamental Theory of Molecular Science; Wiley-VCH Verlag GmbH & Co. KGaA, 2015.
- (18) Greiner, W. Relativistic Quantum Mechanics: Wave Equations; Springer-Verlag Berlin Heidelberg, 1990.
- (19) Zeldovich, Y. B.; Popov, V. S. Electronic Structure of Superheavy Atoms. Sov. Phys. Uspekhi 1972, 14, 673-694.
- (20) Greiner, W.; Reinhardt, J. Quantum Electrodynamics, 3rd ed.; Springer: Berlin, 2003.

- (21) Friedrich, H. Theoretical Atomic Physics, 4th ed.; Springer: Cham, Switzerland, 2017.
- (22) Gamow, G. Mr. Tompkins in Wonderland; or Stories of c, G, and H; The Macmillan Co.: New York, 1940.
- (23) Johnson, W. R. Atomic Structure Theory: Lectures on Atomic Physics; Springer-Verlag: Berlin, 2007.
- (24) Dergachev, V. D.; Nakritskaia, D. D.; Varganov, S. A. Strong Relativistic Effects in Lanthanide-Based Single-Molecule Magnets. *J. Phys. Chem. Lett.* **2022**, *13*, 6749–6754.
- (25) Benner, S. A.; Ricardo, A.; Carrigan, M. A. Is There a Common Chemical Model for Life in the Universe? *Curr. Opin. Chem. Biol.* **2004**, *8*, 672–689.
- (26) Christensen, H. N. Role of Amino Acid Transport and Countertransport in Nutrition and Metabolism. *Physiol. Rev.* **1990**, *70*, 43–77.
- (27) Lodi, L.; Tolchenov, R. N.; Tennyson, J.; Lynas-Gray, A. E.; Shirin, S. V.; Zobov, N. F.; Polyansky, O. L.; Császár, A. G.; Van Stralen, J. N. P.; Visscher, L. A New Ab Initio Ground-State Dipole Moment Surface for the Water Molecule. *J. Chem. Phys.* **2008**, *128*, No. 044304.
- (28) Engel, T.; Reid, P. Physical Chemistry, 3rd ed.; Pearson Education, Inc., 2012.
- (29) Yurchenko, S. N.; Carvajal, M.; Lin, H.; Zheng, J.; Thiel, W.; Jensen, P. Dipole Moment and Rovibrational Intensities in the Electronic Ground State of NH₃: Bridging the Gap between Ab Initio Theory and Spectroscopic Experiment. *J. Chem. Phys.* **2005**, *122*, No. 104317.
- (30) Stillinger, F. H. Water Revisited. Science 1980, 209, 451-457.
- (31) Chang, R. Physical Chemistry for the Biosciences; University Science Books: Sausalito, CA, 2005.
- (32) Roberts, B. M.; Blewitt, G.; Dailey, C.; Murphy, M.; Pospelov, M.; Rollings, A.; Sherman, J.; Williams, W.; Derevianko, A. Search for Domain Wall Dark Matter with Atomic Clocks on Board Global Positioning System Satellites. *Nat. Commun.* **2017**, *8*, 1195.
- (33) Flambaum, V. V.; Kozlov, M. G. Limit on the Cosmological Variation of m_p/m_e from the Inversion Spectrum of Ammonia. *Phys. Rev. Lett.* **2007**, 98, No. 240801.
- (34) Saue, T.; Jensen, H. J. A. Quaternion Symmetry in Relativistic Molecular Calculations: The Dirac-Hartree-Fock Method. *J. Chem. Phys.* **1999**, *111*, 6211–6222.
- (35) Saue, T.; Bast, R.; Gomes, A. S. P.; Jensen, H. J. A.; Visscher, L.; Aucar, I. A.; Di Remigio, R.; Dyall, K. G.; Eliav, E.; Fasshauer, E.; et al. The DIRAC Code for Relativistic Molecular Calculations. *J. Chem. Phys.* **2020**, *152*, No. 204104.
- (36) Peterson, K. A.; Woon, D. E.; Dunning, T. H. J. Benchmark Calculations with Correlated Molecular Wave Functions. IV. The Classical Barrier Height of the $H+H_2\rightarrow H_2+H$ Reaction. *J. Chem. Phys.* **1994**, *100*, 7410–7415.
- (37) Mourik, T.; Van; Wilson, A. K.; Dunning, T. H. J. Benchmark Calculations with Correlated Molecular Wavefunctions. XIII. Potential Energy Curves for He₂, Ne₂ and Ar₂ Using Correlation Consistent Basis Sets through Augmented Sextuple Zeta. *Mol. Phys.* **1999**, *96*, 529–547.

Effect of Extreme Variations of Fundamental Constants on Structure of Atoms and Molecules

Supporting Information

Vsevolod D. Dergachev,¹ Hoang Bao Tran Tan,²,³ Sergey A. Varganov,¹,* and Andrei Derevianko²,†

¹Department of Chemistry, University of Nevada, Reno, 1664 N. Virginia Street, Reno, Nevada 89557-0216, United States

²Department of Physics, University of Nevada, Reno, 1664 N. Virginia Street, Reno, Nevada 89557-0216, United States

³Los Alamos National Laboratory, P.O. Box 1663, Los Alamos, New Mexico 87545, USA

*e-mail: svarganov@unr.edu

†e-mail: andrei@unr.edu

Contents

non-relativistic Born-Oppenheimer approximation
Section II. Critical values of the speed of light for finite-size nuclei
Section III. Effect of varying speed of light on electronic structure of many-electron
atoms
Nitrogen S14
Oxygen
Fluorine
Neon
Section IV. Effect of varying speed of light on electronic structure of water and ammonia
Water S26
Ammonia
Section V. Dipole moments of water and ammonia at the nominal, intermediate, and near
critical values of the speed of light
References

Section I. Invariance of molecular geometry under variation of fundamental constants in the non-relativistic Born-Oppenheimer approximation

The goal of this section is to prove that the effect of variation of fundamental constants cause all the molecular bonds to stretch/dilate by the very same scaling factor, leaving the angles between chemical bonds unaffected, see Figure S1. This statement holds only in the assumption of (i) non-relativistic approximation, (ii) infinitely-heavy nuclei (Born-Oppenheimer approximation) and (iii) point-like spin-less nuclei. If either of these assumptions is broken, chemical bond angles would vary with changing fundamental constants (FCs.)

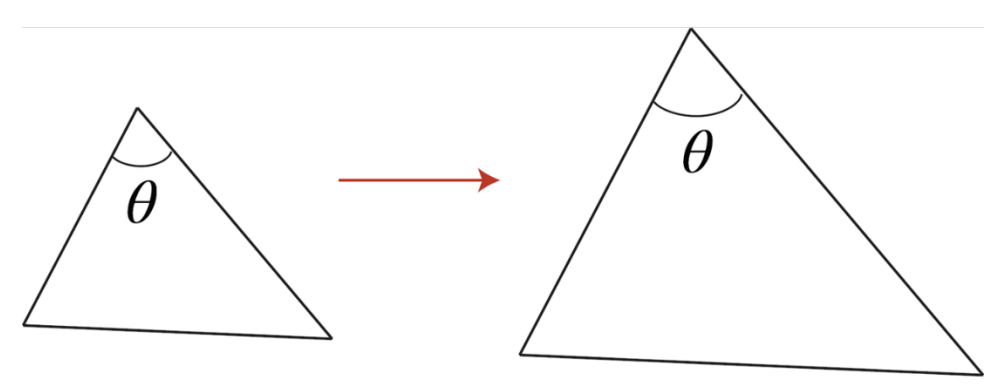


Figure S1. Scaling all the sides of the triangle by the very same numerical factor does not affect the value of angle θ (or of any other angle in the triangle). This example can be generalized to 3D geometry: angles and thus the molecular geometry are not affected by scaling of all the inter-nuclear distances by the same factor (isotropic scaling transformation).

Consider an arbitrary molecule containing N_n point-like nuclei and N_e electrons. Under the enumerated assumptions, the non-relativistic Born-Oppenheimer (NR-BO) Hamiltonian reads

$$H_{\text{NR-BO}} = \sum_{i} -\frac{\hbar^{2}}{2m_{e}} \Delta_{r_{i}} + \frac{1}{2} \sum_{i \neq j} \frac{e^{2}}{|\mathbf{r}_{i} - \mathbf{r}_{j}|} + \frac{1}{2} \sum_{n \neq n'} \frac{Z_{n} Z_{n'} e^{2}}{|\mathbf{R}_{n} - \mathbf{R}_{n'}|} - \sum_{i,n} \frac{Z_{n} e^{2}}{|\mathbf{R}_{n} - \mathbf{r}_{i}|}.$$
 (S1)

Here, for clarity, all FCs are retained. Positions of electrons are labeled as \mathbf{r}_i and those of nuclei – as \mathbf{R}_n . All the terms in $H_{\text{NR-BO}}$ have their usual meaning: kinetic energy of electrons, electron repulsion, nuclear repulsion, and electron-nucleus attraction. Z_n are nuclear charges. To determine the molecular geometry in the Born-Oppenheimer approximation, one solves the time-independent Schrödinger equation with fixed positions of nuclei,

$$H_{\text{NR-BO}}(\mathbf{r}_e|\mathbf{R}_n)\Psi(\mathbf{r}_e|\mathbf{R}_n) = E(\mathbf{R}_n)\Psi(\mathbf{r}_e|\mathbf{R}_n). \tag{S2}$$

Here the Hamiltonian H and thus the eigenfunctions Ψ and energies E depend on fundamental constants: $E(\mathbf{R}_n|m_e,\hbar,e)$. After the potential surfaces $E(\mathbf{R}_n|m_e,\hbar,e)$ are obtained as

functions of nuclear coordinates, the equilibrium nuclear positions, $\{\mathbf{R}_n^{\text{eq}}\}$, are determined by minimizing the energy

$$\min_{\{\mathbf{R}_n\}} E(\mathbf{R}_n | m_e, \hbar, e) \Rightarrow \{\mathbf{R}_n^{\text{eq}}\}. \tag{S3}$$

We would like to explicitly factor out the dependence on FCs from eq S2. We rescale all the coordinates by the same factor ξ : $\mathbf{r}_i \to \xi \boldsymbol{\rho}_i$, $\mathbf{R}_n \to \xi \boldsymbol{\rho}_n$. Upon substitution into $H_{\mathrm{NR-BO}}$, the kinetic energy term transforms into $-\sum_i^{N_e} \frac{\hbar^2}{2m_e\xi^2} \Delta_{\rho_i}$ and all the electrostatic interaction potentials are divided by ξ . We pick the dimension-full pre-factors in the kinetic and potential energy contributions to be equal.

$$\frac{\hbar^2}{m_e \xi^2} = \frac{e^2}{\xi}.\tag{S4}$$

This particular choice enables factoring out the dependence on the FCs from the Hamiltonian *H*. Solving the above equation results in

$$\xi = \frac{\hbar^2}{m_e e^2},\tag{S5}$$

which is the Bohr radius a. Then the Hamiltonian is $H_{NR-BO} = E_h h(\rho_e | \rho_n)$, where

$$E_h = \hbar^2 / m_e \xi^2 = e^2 / \xi = m_e e^4 / \hbar^2$$
 (S6)

is atomic unit of energy (Hartree). Moreover, the scaled Hamiltonian $h(\rho_e|\rho_n)$ no longer depends on FCs. Thereby, the solution of the eigenvalue eq S2

$$h(\boldsymbol{\rho}_e|\boldsymbol{\rho}_n)\varphi(\boldsymbol{\rho}_e|\boldsymbol{\rho}_n) = \varepsilon(\boldsymbol{\rho}_n)\varphi(\boldsymbol{\rho}_e|\boldsymbol{\rho}_n) \tag{S7}$$

does not depend on FCs either. For any value of FCs,

$$E(\mathbf{R}_n|m_e,\hbar,e) = \frac{m_e e^4}{\hbar^2} \varepsilon(\boldsymbol{\rho}_n).$$
 (S8)

Finding equilibrium positions as prescribed by eq S9 also does not depend on FCs,

$$\min_{\{\boldsymbol{\rho}_n\}} \varepsilon(\boldsymbol{\rho}_n) \Rightarrow \{\boldsymbol{\rho}_n^{\text{eq}}\}. \tag{S9}$$

Thereby,

$$\mathbf{R}_n^{\text{eq}} = \frac{\hbar^2}{m_e e^2} \boldsymbol{\rho}_n^{\text{eq}},\tag{S10}$$

where ${m
ho}_n^{
m eq}$ are FC-independent.

To reiterate, in the non-relativistic Born-Oppenheimer approximation, as FCs are varied from their nominal values, all the equilibrium positions are scaled by the very same factor,

$$\mathbf{R}_{n}^{\text{eq}} = \frac{a}{a_0} \mathbf{R}_{n,0}^{\text{eq}}.$$
 (S11)

Here and below all the quantities with the subscript 0 refer to the nominal values. This scaling of all the coordinates by the same factor belongs to the class of isotropic scaling transformations; as such it does not affect molecular bond angles, see Figure S1.

The fact that the isotropic scaling does not affect angles in a molecule of arbitrary geometry can be formally proven as follows. Choose $\{\mathbf{R}_n\}$, $n=\overline{1,N}$ to be (equilibrium) position vectors of all N nuclei in a molecule. The angle θ_{ab} between a pair of these vectors, \mathbf{R}_a and \mathbf{R}_b , is given by

$$\theta_{ab} = \cos^{-1} \left[\frac{(\mathbf{R}_a \cdot \mathbf{R}_b)}{|\mathbf{R}_a| |\mathbf{R}_b|} \right], \tag{S12}$$

where we used the conventional definition of scalar products and $|\mathbf{R}_a| = \sqrt{(\mathbf{R}_a \cdot \mathbf{R}_a)}$ is the length of the vector. Should all the position vectors be scaled by some factor λ , $\mathbf{R}_n \to \lambda \mathbf{R}_n$, the factors of λ in eq S12 cancel out. Thereby, the angles between chemical bonds are not affected by the isotropic scaling. The entire molecule undergoes isotropic stretching or dilation as the FCs are varied.

In addition, as follows from our derivation, all the electron coordinates undergo the same isotropic scaling,

$$\mathbf{r}_e = \frac{a}{a_0} \mathbf{r}_{e,0}. \tag{S13}$$

In particular, it means that the sizes of electronic clouds and atoms are scaled by the same a/a_0 ratio. Another point is that all the energies (both atomic and molecular) are scaled by the atomic unit of energy

$$E = \frac{E_h}{E_{h,0}} E_0. \tag{S14}$$

These observations offer a visualization: as a clump of FCs sweeps through an atom or a molecule, all the energy states are gently modulated and the atoms and molecules "breathe" in accordance with the local values of FCs. This picture is valid in the regime of sufficiently large

and slow FC clumps. The clumps need to be sufficiently large, so there are no gradients of FCs across individual atoms and molecules. The clumps have to be sufficiently slow, so that the induced perturbation does not cause transitions between molecular or atomic states. Then the molecules follow the change in FCs adiabatically.

It is worth emphasizing that our proof heavily relied on the possibility of factoring out all the dependence on FCs in various contributions to the H_{NR-BO} Hamiltonian. If we were to add kinetic energies of the nuclei to H_{NR-BO} , our coordinate scaling procedure would result in the requirement

$$\frac{\hbar^2}{m_e \xi^2} = \frac{e^2}{\xi} = \frac{\hbar^2}{M_1 \xi^2} = \dots = \frac{\hbar^2}{M_N \xi^2},$$
 (S15)

where M_n are nuclear masses. Generically, these equalities cannot be satisfied simultaneously by any choice of the scaling parameter ξ .

Our factorization procedure depended on the fact that the Coulomb interactions in the $H_{\rm NR-BO}$ Hamiltonian exhibited power-law dependence with respect to distances. If the nuclei have finite size, the Hamiltonian no longer admits simple coordinate scaling. Moreover, introducing nuclear properties (such as finite-size charge distribution or hyperfine interactions with nuclear moments) into the problem brings in another FC, $m_q/\Lambda_{\rm QCD}$, where m_q is the average mass of up and down quarks and $\Lambda_{\rm QCD}$ is the energy scale of quantum chromodynamics.

Similarly, Dirac equation does not admit factoring out all the FCs in the Hamiltonian. Indeed, even in the simplest case of hydrogen atom with an infinitely-heavy point-like nucleus, Dirac Hamiltonian contains three terms,

$$h_{\rm D} = -i\hbar c\boldsymbol{\alpha} \cdot \boldsymbol{\nabla} + \beta m_e c^2 - \frac{e^2}{r}.$$
 (S16)

Since the 4 × 4 Dirac matrices α and β are collections of FC-independent complex numbers, our coordinate scaling procedure results in the requirement

$$\frac{\hbar c}{\xi} = m_e c^2 = \frac{e^2}{\xi}.\tag{S17}$$

For arbitrary values of FCs $(m_e, \hbar, e, \text{ and } c)$, these equalities are mutually exclusive. We conclude that relativity must lead to the breakdown of the isotropic scaling of atomic structure and molecular geometry with varying FCs. Chemical bond angles vary with changing FCs due to relativistic effects.

Since the theory of quantum electrodynamics (QED) is built on quantizing relativistic fields, field-theoretic effects also lead to the breakdown of the isotropic scaling with varying FCs. This can be easily seen by examining effects of vacuum polarization by the nucleus¹. In QED, a nucleus is immersed into a nuclear-field-polarized cloud of virtual pairs of particles and anti-particles. Vacuum polarization leads to the replacement of the -Z/r Coulomb

potential of a point-like nucleus by the Uehling potential. The success of our factorization procedure depends on the fact that the Coulomb interactions in the NR-BO Hamiltonian exhibits a power-law dependence with respect to distances. The Uehling potential lacks this power-law dependence and, thereby, does not admit factoring out FCs in the resulting Hamiltonian.

Scaling of molecular geometry preserves angles between chemical bonds in the NR-BO approximation. Molecular geometry "breathes" with varying FCs. Consider a thought experiment where we compare lengths of two rulers of different chemical composition. Suppose at the nominal values of FCs both rulers have the same lengths. As the FCs change, both rulers are expanding/contracting by the same factor in the NR-BO approximation. The observer would not be able to tell if FCs have changed. The very same argument applies to transition frequency comparisons: in the NR-BO approximation, all the dependence of energies on FCs is governed by the common factor of Hartree energy $m_e e^4/\hbar^2$. Corrections to the most basic NR-BO approximation violate this isotropic scaling law: the lengths of two rulers in our though experiment would differ for varying FCs. Similarly, the ratios of transition frequencies for two different atoms or molecules would change with varying FCs.

Section II. Critical values of the speed of light for finite-size nuclei

In this section, for convenience we focus on the fine-structure constant α instead of the speed of light c. The main results inferred for α can be easily converted to those of c via the reciprocal relation $\alpha=1/c$. The critical value α^* of varying electromagnetic fine structure constant α is determined by the requirement that the energy ε of the bound electron becomes equal to the Dirac sea threshold, $\varepsilon=-2m_ec^2$. Here and below the energy excludes the rest mass energy. This problem can be solved analytically^{1,2}, where the authors were interested in determining the critical nuclear charge value for the fixed nominal value of α .

The analytical solution can be developed for nuclear spherical shell-like charge density distribution, $\rho_{\rm shell}(r) \propto \delta(r-R)$, where R is the radius of the nuclear charge shell. Qualitatively, inside the nuclear shell, r < R, the potential is constant $V(r) = -Ze^2/R$ and the solution to the Dirac equation is given by the energy-offset free particle solutions. Outside the nuclear shell, the potential is of the Coulomb character, $V(r) = -Ze^2/r$, and the solution to the Dirac equation is given by the linear combinations of the regular and irregular Coulomb wavefunctions. Setting $\varepsilon = -2m_e c^2$ and matching the inner and outer solutions at r = R leads to a transcendental equation for α^*

$$\xi \frac{K'_{i\nu}(\xi)}{K_{i\nu}(\xi)} = 2(\alpha^* Z)\cot(\alpha^* Z), \tag{S18}$$

where $\xi = \sqrt{8ZR/\alpha_0}$, $K_{i\nu}(\xi)$ is the modified Bessel function of the second kind (Macdonald function) with index $\nu \equiv 2\sqrt{(\alpha^*Z)^2 - 1}$ with $K'_{i\nu}(\xi)$ being its derivative with respect to ξ . Eq S18 is specific to the $ns_{1/2}$ orbitals. Subsequently increasing roots of this equation corresponds to larger values of principle quantum number n. Similar equations can be derived for orbitals of larger total angular momenta.

To solve eq S18, we need to specify the spherical shell radius R. We make the connection to the more realistic nuclear charge distributions by noticing that for the spherical shell distribution, the r.m.s. radius $R_{\rm rms}$ is identical to R. For proton, we take the 2018 CODATA³ recommended value, $R_{\rm rms}(^{1}{\rm H}) = 0.8414(19)$ fm. For heavier elements, we use an approximation $^{1}R \approx 1.6Z^{1/3}$ fm, adequate for our discussions.

From eq S18 we find the critical value of α for hydrogen $1s_{1/2}$ orbital occurs at $\alpha^{\star} \approx 1.04$ or $c^{\star} \approx c_0/143$. One may argue that the spherical shell approximation for the nuclear charge distributions used in deriving eq S18 is not realistic. To address this question, we solved the Dirac equation for hydrogen using numerical finite-differencing techniques⁴; for the uniform nuclear charge distribution we find $\alpha^{\star} \approx 1.042$. This is to be compared to the spherical shell result of 1.040. A similar exercise for Fermium (Z=100, A=257, $R_{\rm rms}=7.1717$ fm) shows that $1s_{1/2}$ α^{\star} for the spherical shell distribution is 1.20×10^{-2} versus 1.18×10^{-2} for both the uniform and the Fermi nuclear charge distributions. Thereby, more realistic models of charge distributions lead to somewhat smaller values of α^{\star} than those resulting from the spherical shell distribution.

We notice that Dirac code internally uses Gaussian nuclear charge distributions with $R_{\rm rms}$ given by the fitting formula⁵

$$R_{\rm rms} = 0.836A^{1/3} + 0.570(\pm 0.05) \,\text{fm}.$$
 (S19)

For a given charge Z we use the most abundant isotope mass number A. This formula results in the proton $R_{\rm rms}(^1{\rm H}) = 1.406$ fm which is almost as twice as large than the CODATA recommended value, $R_{\rm rms}(^1{\rm H}) = 0.8414(19)$ fm. The simple reason for this discrepancy is that eq S19 is a fit for atomic mass numbers A > 9.5 If we use the value $R_{\rm rms}(^1{\rm H}) = 1.406$ fm, eq S18 results in $\alpha^*(^1{\rm H}) = 1.044$, slightly larger than the value of 1.040 obtained with the CODATA $R_{\rm rms}(^1{\rm H})$.

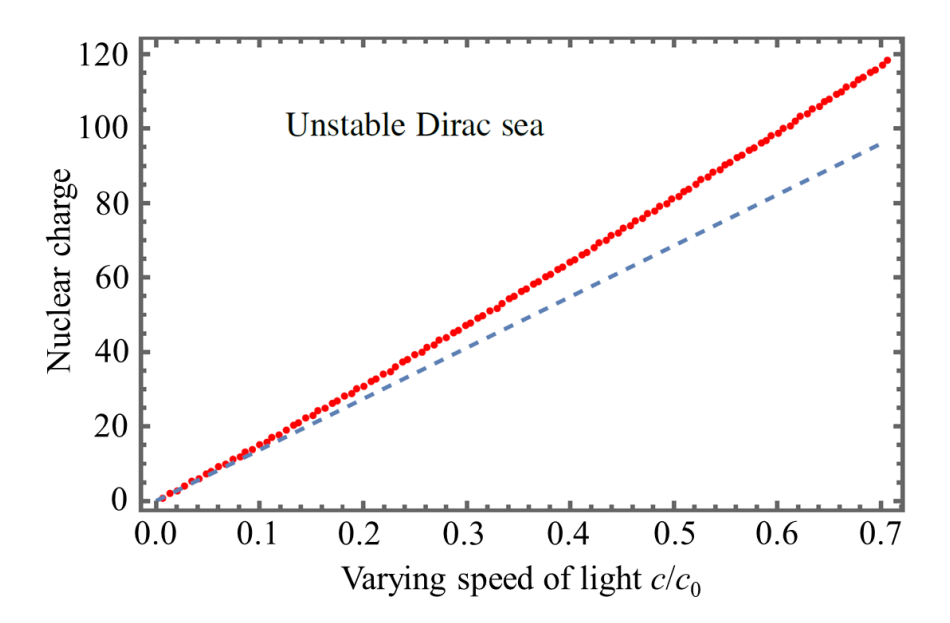


Figure S2. Phase diagram of periodic system of elements as a function of varying speed of light. Red and blue curves are the results for critical values of c^*/c_0 as a function of nuclear charge Z for finite-size and point-like nuclei, respectively. To borrow an analogy from condensed matter physics, α (or c) is an order parameter that governs phase transitions.

The results of our calculations are shown in Figure S2. In this plot, the red curve are the results for critical values of c^*/c_0 as a function of nuclear charge Z for finite-size nuclei. Blue curve is the same dependence but for point-like nuclei, $\alpha^* = 1/Z$. This parameter space can be interpreted as a phase diagram: any point $(c/c_0, Z)$ above the red curve corresponds to unstable Dirac sea. Here, for comparison, we also plot the critical values for point-like nucleus, $Z_{\text{max}} = 1/\alpha^*$, i.e. $Z_{\text{max}} = \alpha_0 c^*/c_0$.

Finite-size nuclei critical curve exhibit nearly linear dependence with a fit,

$$Z_{\text{max}} \approx 168c/c_0. \tag{S20}$$

The nearly linear dependence can be understood by examining the graphical solution of transcendental eq S18, see Figure S3 for hydrogen. Plots for heavier elements are similar. Even without solving the eq S18, it is apparent that the critical value of α for the $1s_{1/2}$ orbital occurs in the vicinity of the first zero of Macdonald function $K_{i\nu}(\xi)$, where the l.h.s. approaches vertical asymptote. The first zero of $K_{i\nu}(\xi)$ is given by $\ln \xi \approx -\pi/\nu + \ln 2 - \gamma_{\rm Euler}$, where $\gamma_{\rm Euler} = 0.5772156649...$ is the Euler constant. This leads to an analytical estimate

$$\alpha^{\star} \lesssim \frac{1}{Z} \left(1 + \frac{\pi^2}{8} \frac{1}{\left(\gamma_{\text{Euler}} + \frac{1}{2} \ln \left(\frac{\sqrt{2}ZR}{a_0} \right)^2 \right)} \right).$$
 (S21)

The leading 1/Z term can be recognized as the critical value for point-like nucleus. We use the smaller sign (\lesssim) because the true value of α^* lies below this asymptotic estimate, see Figure S3. The fractional contribution of the corrective term has a weak logarithmic dependence on the nuclear charge, $\ln(Z^{4/3})$, explaining the nearly linear dependence of maximum allowed nuclear charge in Figure S2. In approximate eq S21 we also restored the Bohr radius a_0 , showing that the dominant dependence is the ratio of nuclear radius R to the characteristic size of atomic orbital a_0/Z . Approximation as per eq S21 tends to overestimate α^* . Its relative accuracy ranges from 2% for hydrogen to 50% for Fermium (Z = 100) as follows from comparison with our numerical results. Quantum electro-dynamics (QED) corrections to the $1s_{1/2}$ energy (vacuum polarization and self-energy) tend to cancel¹, leaving critical values largely unaffected.

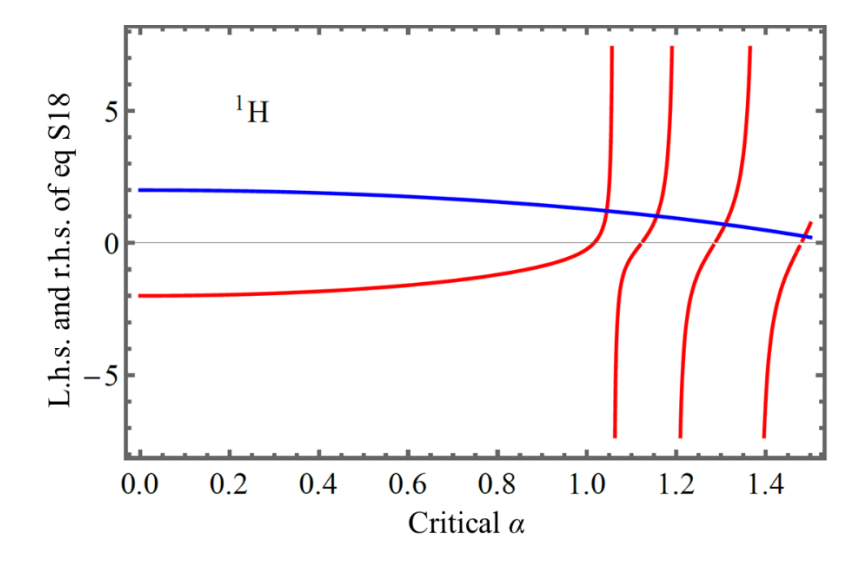


Figure S3. Graphical determination of critical values of fine-structure constant for hydrogen (Z=1,R=0.8414 fm). The r.h.s. and the l.h.s of transcendental eq S18 are drawn as red and blue curves, respectively. The values of α at the intersection of two curves are critical values α^* of α . The lowest α^* is the critical value for $1s_{1/2}$, next lowest α^* is for $2s_{1/2}$ and so on.

For multi-electron systems, the stability of an atom with respect to varying FCs requires further qualifiers. Indeed, unlike in H-like ions, a Dirac sea electron cannot transition into the fully occupied $1s_{1/2}$ orbital due to the Pauli exclusion principle.² Yet, because the rest-mass energy gap is lowered, background photons can promote Dirac sea electrons into unoccupied orbitals, i.e., Dirac sea becomes unstable with respect to the interaction with photon bath. As to the critical values, we computed Dirac-Hartree-Fock energies of $1s_{1/2}$ orbitals in several atoms as a function of c. We find that the hydrogen-like ion result per eq 1 of the main text remains a good approximation for c^* . Indeed, energies of the deeply-bound $1s_{1/2}$ orbitals in atoms and molecules are strongly dominated by the interaction with the nucleus with small corrections from the interaction with other electrons.

Section III. Effect of varying speed of light on electronic structure of manyelectron atoms

The atomic spectra of N, O, F, and Ne atoms were calculated at different values of the speed of light (or α) using the Kramer Restricted Configuration Interaction (KRCI) method, as implemented in DIRAC19.^{7,8} The Dirac-Hartree-Fock (DHF) calculations were first carried out to obtain the reference wavefunction for the CI step. In the DHF calculations, the $3s_{1/2}$ orbital was included in the active space via the average-of-configuration open-shell framework. This ensures the balanced description of atomic states at the CI step and allows us to assess the effects of the relativistic stabilization of the $3s_{1/2}$ orbital. At the nominal c, the atomic states are labeled in the conventional L-S (Russell-Saunders) coupling scheme: ^{2S+1}L_J, where S is the total spin, L is the orbital angular momentum, and J is the total angular momentum. At decreased c, however, the amplified relativity leads to the breakdown of the LS coupling scheme, as only the total angular momentum J, J = L + S, is conserved.⁴ Thereby, we label the states as J^{π} , where J is the value of the total angular momentum and π is the parity of the state. If there are multiple states of the same J^{π} symmetry, we distinguish them by appending their sequential number n: J^{π} (n), where the states are enumerated in the order of increasing energy. In our notation for electronic configurations, for brevity, we suppress the $1s_{1/2}$ and $2s_{1/2}$ shells, as these remain always doubly occupied for our considered low-lying energy states.

Since the typical distance of an electron from the nucleus decreases with c due to relativistic contraction, the basis sets used in our calculations needed to be calibrated to accurately describe the electronic density near the nucleus at reduced c. The calibrating procedure was carried out by considering the hydrogen-like ions of N, O, F, and Ne as follows. For a selected ion, the speed of light was gradually lowered until the $1s_{1/2}$ ground state dived into the Dirac sea. The size of the basis set and the largest exponents were chosen to match the critical values of c^* obtained using such a basis set with that predicted by solving the transcendental eq S18. Additionally, the validity of these basis sets was verified by comparing the energy level orderings they generated with those predicted by the finite-difference solution of the Dirac equation. To obtain the correct energy ordering, it required to augment standard basis sets with additional p basis functions.

For example, for N, the eleven p basis functions in the original uncontracted aug-cc-pV6Z basis set were augmented to a total of nineteen. The exponents of the new functions were obtained by subsequently multiplying the largest p exponent by 3. For simplicity, the same exponents were used for the s basis functions. This procedure was carried out until a match with the solution to the transcendental eq S18 was obtained, while maintaining the correct ordering of the energy levels. The resulting modified basis thus included nineteen s and nineteen p basis functions with the largest exponent being 6.9×10^8 . The basis functions of higher angular momenta were left unchanged. The same strategy was used for O, F, and Ne, yielding modified basis sets containing also nineteen s and nineteen s basis functions. The largest exponents were, respectively, s0 or 0, s1.1 × 10 or 0, s2 for F, and s3. With such modified basis sets, the critical s5 values obtained using the DIRAC19 program

matched those predicted by eq S17, namely, the critical values are $c_{\rm N}^{\star} \approx c_0/21.1$, $c_{\rm O}^{\star} \approx c_0/18.4$, $c_{\rm F}^{\star} \approx c_0/16.4$, and $c_{\rm Ne}^{\star} \approx c_0/14.8$.

To avoid the collapse of the many-electron wavefunction into the Dirac sea,⁹ the so-called 'no-pair' Hamiltonian^{10,11} was used in fully relativistic electronic structure calculations

$$H_{\text{no-pair}} = \sum_{i} h_{D}(i) + \frac{1}{2} \sum_{i \neq j} \Lambda_{++} \frac{1}{r_{ij}} \Lambda_{++}, \tag{S22}$$

where the first term is the sum of the Dirac Hamiltonian $h_D(i)$ describing an electron i moving in the potential of a finite-size nucleus and the second term describes the Coulomb repulsion between the electrons. The e-e interaction is sandwiched between the projection operators Λ_{++} which exclude states from the Dirac sea continuum of h_D .

We have described the methods with which we computed the low-lying energy states of several second-period atoms, from nitrogen through to neon, at the nominal and reduced speeds of light. Below, we present the results of our calculations. We find that as c is reduced, the energies of the excited states of an atom exhibit various interesting features. Relative to the energy of the 'nominal' ground state (the ground state at nominal c), an excited state energy may rise or fall in the regime $c \sim c_0/10$, leading to several crossings of levels. However, as c is reduced further, all excited states eventually stabilize with respect to the nominal ground state. Even more remarkably, as c nears c^* , the energies of some excited states decrease so much that these states become the 'new' ground states themselves. This phenomenon happens in all considered atoms, albeit to different degrees: in F, the change in the nature of the ground state only lasts for a small interval of c around $c_0/15$, whereas in N, O, and Ne, the 'usurping' excited states remain the ground state of their respective atoms until c reaches c^* .

We show below that the electron-configuration picture is sufficient for the qualitative explanation of these phenomena. The lynch-pins of this exposition are the facts that as c decreases, (i) the $2p_{1/2}$ energy decreases, (ii) the $2p_{3/2}$ energy increases, (iii) the $3p_{1/2}$ energy falls, but with a slower rate than that of $2p_{1/2}$, (iv) the $3p_{3/2}$ energy rises but with a slower rate than that of $2p_{3/2}$, and (v) all $s_{1/2}$ energies fall. It is worth stressing that the rise in the energy of $2p_{3/2}$ (and similarly of all other $p_{3/2}$) orbitals is only present in multi-electron atoms. In a hydrogen-like atom, although the fine-structure contribution to a $2p_{3/2}$ energy increases with decreasing c, the gross-structure contribution decreases (it is a negative quantity whose magnitude gets larger), leading to an overall decline of the $2p_{3/2}$ energy. In a multi-electron atom, however, the contractions of the inner $1s_{1/2}$, $2s_{1/2}$, and $2p_{1/2}$ orbitals with decreasing c leads to more effective screening of the nuclear charge, thus reducing the magnitude of the gross-structure contribution to the $2p_{3/2}$ energy. This in turn means that the $2p_{3/2}$ energy increases with decreasing c.

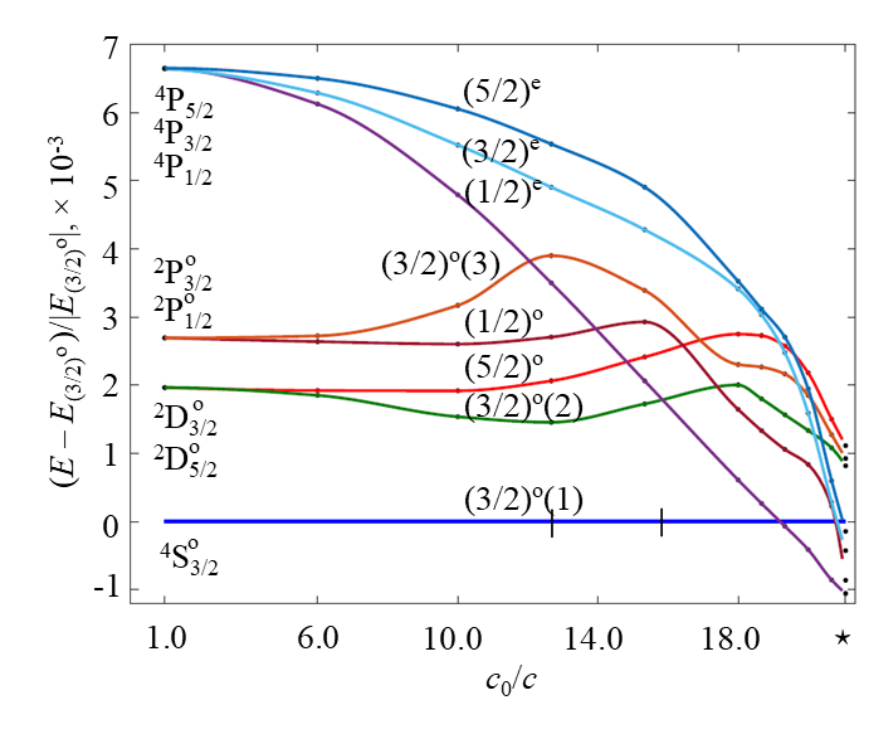


Figure S4. Energy spectrum of a nitrogen atom as a function of the speed of light (or α). The critical value of c_0/c is marked with star (\star).

We begin our discussion with the nitrogen atom, describing the changes in its eight lowest energy states induced by varying c (Figure S4). The $2p^3$ ground electron configuration of the nitrogen atom produces five states arising from all possible distributions of three valence electrons over the six spin-orbitals $2p_{1/2,\pm 1/2}$, $2p_{3/2,\pm 1/2}$ and $2p_{3/2,\pm 3/2}$. The ground state, labeled as $^4S^o_{3/2}$ at $c=c_0$, is the spin quartet with the total orbital angular momentum L=0. The left superscript is the spin multiplicity 2S+1, and the right superscript o indicates an odd parity.

The excited states of the $2p^3$ configuration at the nominal c are the spin doublet states ${}^2D^o$ and ${}^2P^o$, with orbital angular momenta L=2 and L=1, respectively. The ${}^2D^o$ and ${}^2P^o$ states both split into the components with different values of the total angular momentum quantum number J. Namely, the ${}^2D^o$ state splits into ${}^2D^o_{5/2}$ and ${}^2D^o_{3/2}$, whereas ${}^2P^o$ state – into the ${}^2P^o_{1/2}$ and ${}^2P^o_{3/2}$ states. The first excited configuration $2p^23s$ produces the following quartet states of even parity: ${}^4P_{1/2}$, ${}^4P_{3/2}$ and ${}^4P_{5/2}$.

At $c < c_0$, the eight states are labeled as $(3/2)^{\circ}(1)$, $(5/2)^{\circ}$, $(3/2)^{\circ}(2)$, $(1/2)^{\circ}$, $(3/2)^{\circ}(3)$, $(1/2)^{e}$, and $(5/2)^{e}$, respectively, using the J^{π} notation. Throughout this discussion, the nominal ground state $(3/2)^{\circ}(1)$, which corresponds to ${}^{4}S_{3/2}^{\circ}$ at nominal c, is used as a reference; and all state energies are reported as the ratio $(E - E_{(3/2)^{\circ}})/|E_{(3/2)^{\circ}}|$.

This choice does not imply, however, that the energy of $(3/2)^{o}(1)$ remains unaffected as c decreases. In fact, the dominant electronic configuration of $(3/2)^{o}(1)$ changes twice within the

range $c^* \le c < c_0$. In the range $c_0/13 \le c < c_0$, the dominant configurations are $2p_{1/2}^2 2p_{3/2}$, $2p_{1/2} 2p_{3/2}^2$ and $2p_{3/2}^3$. As c decreases, the energy of the $2p_{1/2}$ orbital decreases while that of $2p_{3/2}$ increases¹³ until, at $c \le c_0/13$, the $2p_{3/2}^3$ configuration becomes energetically unfavorable and no longer contributes to the ground state. Furthermore, since the $3p_{3/2}$ orbital is further away from the nucleus than the $2p_{3/2}$ orbital, the former is less influenced by relativistic effects than the latter (recall that, at least in the regime of small α , the spin-orbit splitting scales as n^{-3} where n is the principle quantum number). As a result, the $2p_{1/2}2p_{3/2}^2$ configuration eventually becomes less energetically favorable than, and is thus replaced by $2p_{1/2}^22p_{3/2}$. This happens at $c \approx c_0/15$. We now discuss the behavior of the four components of the $^2D^0$ and $^2P^0$ doublets with respect to changing c.

For $c_0/13 \lesssim c < c_0$, the state $(3/2)^{\rm o}(2)$ has dominant configurations $2p_{1/2}2p_{3/2}^2$ and $2p_{1/2}^22p_{3/2}$ whereas the ground state contains the extra $2p_{3/2}^3$. Since the $2p_{3/2}^3$ energy increases with decreasing c, this leads to a slight stabilization of $(3/2)^{\rm o}(2)$ with respect to the ground state. For $c_0/18 \lesssim c < c_0/13$, however, the configuration $2p_{3/2}^3$ drops off from the ground state and $2p_{1/2}^22p_{3/2}$ drops off from $(3/2)^{\rm o}(2)$, leading to the destabilization of $(3/2)^{\rm o}(2)$. At $c \approx c_0/18$, however, an avoided crossing happens between $(3/2)^{\rm o}(2)$ and $(3/2)^{\rm o}(3)$, at which point the dominant configuration of $(3/2)^{\rm o}(2)$ becomes $2p_{1/2}^23p_{3/2}$ and remains so thereafter. This is to be compared with the ground state, whose composition involves $2p_{1/2}^23p_{3/2}$ and $2p_{1/2}^22p_{3/2}$. Since the $3p_{3/2}$ energy increases at a much slower rate than that of $2p_{3/2}$, this results in the eventual stabilization of $(3/2)^{\rm o}(2)$ with respect to the ground state.

Next, we discuss the state $(5/2)^{\circ}$, whose dominant configuration $2p_{1/2}2p_{3/2}^2$ remains the same throughout the variation of c. In the regime $c_0/13.0 \le c < c_0$, the $(5/2)^{\circ}$ energy remains stable relative to that of the ground state $(3/2)^{\circ}(1)$ due to the balance between the $2p_{1/2}^22p_{3/2}$ and $2p_{3/2}^3$ configurations in the latter. However, as soon as $2p_{3/2}^3$ drops off from $(3/2)^{\circ}(1)$ at $c \approx c_0/13$, the state $(5/2)^{\circ}$ starts to destabilize relative to the ground state. This trend continues past $c \approx c_0/15$, where the ground state composition changes to $2p_{1/2}^22p_{3/2}$ and $2p_{1/2}^23p_{3/2}$, until $c \approx c_0/18$, at which point correlation effects, especially interactions with higher-lying states of the same J and parity, force the $(5/2)^{\circ}$ energy down. This results in the stabilization of $(5/2)^{\circ}$ relative to the ground state for $c \leq c_0/18$.

Before describing the behavior of the remaining two states of the $^2D^o$ and $^2P^o$ doublets, we note that the $(5/2)^o$ and $(3/2)^o(2)$ states cross at $c \approx c_0/3$. At the nominal c, $(5/2)^o$ is around 8 cm⁻¹ lower in energy than $(3/2)^o(2)$. In the region $c_0/7 \le c < c_0$, both states are dominated by the $2p_{1/2}2p_{3/2}^2$ configuration. However, the $(3/2)^o(2)$ state, due to its lower value of J, contains a second dominant configuration, $2p_{1/2}^22p_{3/2}$. As c decreases, this extra configuration is responsible for the stabilization of $(3/2)^o(2)$ relative to $(5/2)^o$.

We now turn our attention to the state $(1/2)^{\circ}$. In the regime $c_0/15 \lesssim c < c_0$, its dominant configuration is $2p_{1/2}2p_{3/2}^2$, the same as for $(5/2)^{\circ}$. As a result, the $(1/2)^{\circ}$ energy behaves in a similar way as that of $(5/2)^{\circ}$: relative to the ground state energy, it remains stable for $c_0/13 \lesssim c < c_0$ and rises for $c_0/15 \lesssim c \leq c_0/13$. At $c \approx c_0/15$, however, the avoided

crossing with a higher (nominally) $S_{1/2}^{0}$ state causes the configuration of $(1/2)^{0}$ to become $2p_{1/2}^{2}3p_{1/2}$, which results in $(1/2)^{0}$ rapidly stabilizing with respect to the ground state.

Finally, we discuss the state $(3/2)^{\circ}(3)$. For $c_0/6 \lesssim c \leq c_0$, the dominant configuration in $(3/2)^{\circ}(3)$ is $2p_{1/2}^22p_{3/2}$ with a small mixture of $2p_{3/2}^3$. As a result, in this regime, the energy of $(3/2)^{\circ}(3)$ remains stable relative to that of the ground state $(3/2)^{\circ}(1)$. As c decreases further, the contributions from $2p_{3/2}^3$ to $(3/2)^{\circ}(3)$ grows and eventually becomes dominant, leading to a rapid destabilization of $(3/2)^{\circ}(3)$ with respect to $(3/2)^{\circ}(1)$. One would expect this destabilization to accelerate when c decreases past the value $c_0/13$, whereupon $2p_{3/2}^3$ drops off from the ground state configuration. However, at $c \approx c_0/13$, the avoided crossing between $(3/2)^{\circ}(3)$ and the higher lying $(3/2)^{\circ}(4)$ changes the dominant configuration of $(3/2)^{\circ}(3)$ to $2p_{1/2}^23p_{3/2}$. This leads to a rapid downturn of the $(3/2)^{\circ}(3)$ energy relative to that of $(3/2)^{\circ}(1)$. As noted above, at $c \approx c_0/18$, another avoided crossing, this time between $(3/2)^{\circ}(3)$ and $(3/2)^{\circ}(2)$, occurs, changing the nature of $(3/2)^{\circ}(3)$ to $2p_{1/2}2p_{3/2}^2$. As c decreases, the 'new' state $(3/2)^{\circ}(3)$ stabilizes further due to correlation effects.

We have described the behaviors of the four lowest excited odd-parity states as c varies. We now extend our discussion to the three lowest even-parity states $(1/2)^e$, $(3/2)^e$, and $(5/2)^e$ states, which at the nominal c correspond to ${}^4P_{1/2}$, ${}^4P_{3/2}$, and ${}^4P_{5/2}$. For this purpose, apart from the observation that the $2p_{1/2}$ energy decreases while the $2p_{3/2}$ energy increases as c is reduced, we also need the fact that the $3s_{1/2}$ energy decreases with decreasing c. 12

We begin with the state $(1/2)^e$. Near the nominal c, it comprises of the $2p_{1/2}^2 3s_{1/2}$, $2p_{3/2}^2 3s_{1/2}$, and $2p_{1/2} 2p_{3/2} 3s_{1/2}$ configurations. As c decreases, the destabilizing $2p_{3/2}$ orbital causes the last two configurations to drop off, at $c \approx c_0/10$. The remaining configuration $2p_{1/2}^2 3s_{1/2}$, which contains only stabilizing orbitals, causes the $(1/2)^e$ energy to decline rapidly, until $c \approx c_0/19$, where it falls below the energy of $(3/2)^o(1)$ and $(1/2)^e$ becomes the new ground state of nitrogen.

Similarly, at $c=c_0$, $(3/2)^e$ and $(5/2)^e$ are mixtures of the $2p_{3/2}^23s_{1/2}$ and $2p_{1/2}2p_{3/2}3s_{1/2}$ configurations, with $2p_{3/2}^23s_{1/2}$ dropping off at $c \leq c_0/15$. That these two states have the same dominant configuration for $c \leq c_0/15$ is evident via the near coincidence of the two corresponding curves in this regime, see Figure S4. That their dominant configuration for small c still contains the destabilizing orbital $2p_{3/2}$ also explains why the $(3/2)^e$ and $(5/2)^e$ energies do not decline as fast as that of $(1/2)^e$. As a result, although their energies do fall below that of the nominal ground state $(3/2)^o(1)$, $(3/2)^e$ and $(5/2)^e$ lose out in the competition with $(1/2)^e$ to become the new ground state of nitrogen.

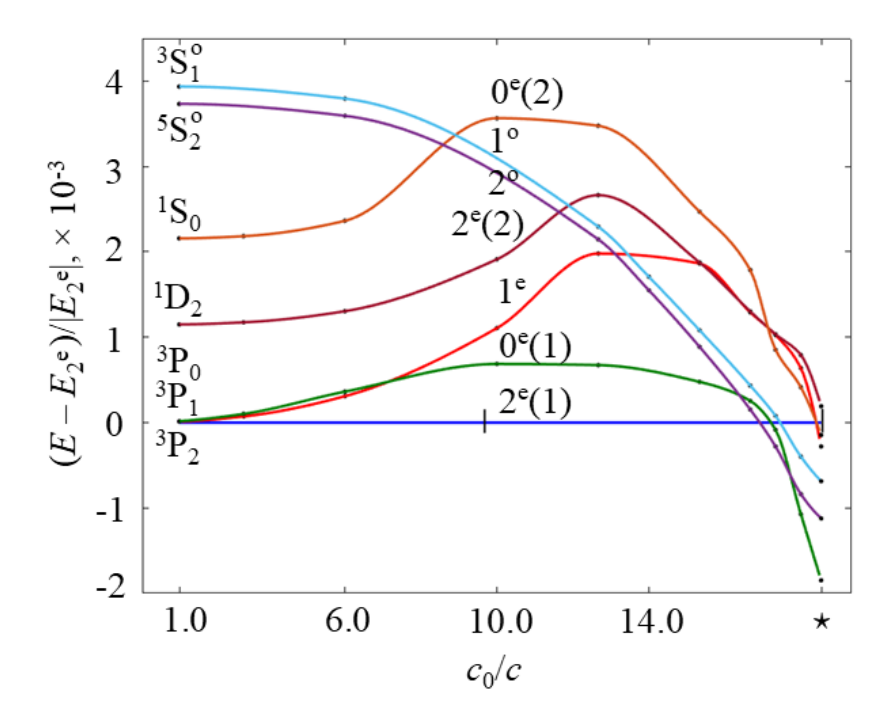


Figure S5. Energy spectrum of an oxygen atom as a function of speed of light (or α). The critical value of c_0/c is marked with star (\star).

In this subsection, we turn to the discussion of the oxygen atom, where we consider five lowest states of even parity, ${}^{3}P_{2}$, ${}^{3}P_{1}$, ${}^{3}P_{0}$, ${}^{1}D_{2}$, and ${}^{1}S_{0}$, originating from the $2p^{4}$ ground electron configuration of oxygen, and the two lowest odd-parity excited states ${}^{5}S_{2}^{0}$ and ${}^{3}S_{1}^{0}$, originating from the $2p^{3}3s$ configuration (Figure S5). The nominal ground state of oxygen, labeled as ${}^{3}P_{2}$ at $c=c_{0}$ and $2^{e}(1)$ for $c< c_{0}$, is used as a reference.

Just like for nitrogen, we begin by describing the behavior of the nominal ground state with decreasing c. In the regime $c_0/10 \lesssim c \leq c_0$, $2^{\rm e}(1)$ comprises predominantly $2p_{1/2}^22p_{3/2}^2$ and $2p_{1/2}2p_{3/2}^3$. For $c \lesssim c_0/10.0$, the $2p_{3/2}$ energy rises high enough so that the contribution of $2p_{1/2}2p_{3/2}^3$ becomes subdominant. At $c \approx c^* \approx c_0/18.4$, the energies of the stabilizing orbital $3s_{1/2}$ and that of the destabilizing orbital $2p_{3/2}$ become nearly degenerate. As a result, two p-shell electrons may be promoted to the $3s_{1/2}$ shell and $2p_{1/2}2p_{3/2}3s_{1/2}^2$ emerges as a dominant configuration in $2^{\rm e}(1)$. Note that this promotion involves one $2p_{1/2}$ and one $2p_{3/2}$ electron due to conservation of the total angular momentum and parity.

Next, we concentrate on the excited states. For $c_0/10 \lesssim c \leq c_0$, the state $0^e(1)$, which at $c=c_0$ is labeled 3P_0 , is a mixture of $2p_{1/2}^22p_{3/2}^2$ and $2p_{3/2}^4$. Since $0^e(1)$ contains a configuration which has a destabilizing orbital $2p_{3/2}$ quadruply occupied, in contrast to $2^e(1)$, in whose configurations $2p_{3/2}$ is at most triply occupied, $0^e(1)$ destabilizes relative to the ground state in this regime. For $c < c_0/10$, the contribution $2p_{3/2}^4$ is no longer significant, leaving only $2p_{1/2}^22p_{3/2}^2$ as the dominant configuration in the CI expansion of $0^e(1)$, similar to

 $2^{\rm e}(1)$. This explains the flattening out of the $0^{\rm e}(1)$ curve in the regime $c_0/13 \lesssim c \lesssim c_0/10$. For $c \lesssim c_0/13$, however, the state $0^{\rm e}(1)$ begins to stabilize relative to the ground state. This is due to the avoided crossing with $0^{\rm e}(2)$, which introduces the configuration $2p_{1/2}^23s_{1/2}^2$ to the CI expansion of $0^{\rm e}(1)$. The doubly-occupied stabilizing $3s_{1/2}$ orbital causes the $0^{\rm e}(1)$ energy to decline rapidly and eventually fall below that of $2^{\rm e}(1)$ at $c \approx c_0/17$, making $0^{\rm e}(1)$ the new ground state of oxygen.

We now address the state 1^e , which at $c=c_0$ is labeled 3P_1 . For $c_0/13 \lesssim c \leq c_0$, the dominant configuration of 1^e is $2p_{1/2}2p_{3/2}^3$, which means that this state destabilizes relative to the nominal ground state (the rate of destabilization increases after $c \approx c_0/10$, when $2p_{1/2}2p_{3/2}^3$ is no longer a dominant contribution to the ground state). However, at $c \approx c_0/13$, the energy of $3p_{1/2}$ is lowered enough so that the configuration $2p_{1/2}^22p_{3/2}3p_{1/2}$ emerges in the expansion of 1^e . Notice that the transfer of one $2p_{3/2}$ electron to the $3p_{1/2}$ shell is accompanied by the demotion of another $2p_{3/2}$ electron to the $2p_{1/2}$ shell in order to conserve total angular momentum. The stabilizing orbital $3p_{1/2}$ causes the 1^e energy to decrease relative to and eventually become lower than that of the nominal ground state. However, the stabilization effect of the singly-occupied $3p_{1/2}$ orbital is not as strong as that of the doubly-occupied $3s_{1/2}$ orbital so 1^e never becomes the new ground state in place of $0^e(1)$.

Before discussing the remaining states, we note that similar to nitrogen, there occurs an 'early' crossing between the $1^{\rm e}$ and $0^{\rm e}(1)$ states of the oxygen atom (Figure S5). At $c=c_0$, $0^{\rm e}(1)$ lies 65 cm⁻¹ higher in energy than $1^{\rm e}$. At $c\approx c_0/7$, the role of $2p_{3/2}^4$ in $0^{\rm e}(1)$ starts to diminish and since the remaining configuration $2p_{1/2}^22p_{3/2}^2$ of $0^{\rm e}(1)$ is more energetically favorable than the $2p_{1/2}2p_{3/2}^3$ of $1^{\rm e}$, $0^{\rm e}(1)$ crosses below $1^{\rm e}$.

We continue our discussion with the state $2^{\rm e}(2)$ which is labeled $^{\rm 1}D_2$ at $c=c_0$. In the regime $c_0/10 \lesssim c \leq c_0$, $2^{\rm e}(2)$ is made up of $2p_{1/2}^22p_{3/2}^2$ and $2p_{1/2}2p_{3/2}^3$, similar to the ground state $2^{\rm e}(1)$, albeit with different proportions of the configurations. As c decreases, the $2p_{1/2}2p_{3/2}^3$ component becomes more and more pronounced in $2^{\rm e}(2)$ instead of fading out as in $2^{\rm e}(1)$. At $c \approx c_0/10$, $2p_{1/2}2p_{3/2}^3$ drops off from the ground state configuration whereas it becomes the dominant contribution to $2^{\rm e}(2)$. These two observations are supported by the upturn of the $2^{\rm e}(2)$ curve relative to the ground state baseline. At $c \approx c_0/13$, however, $2^{\rm e}(2)$ participates in an avoided crossing with the $2^{\rm e}(3)$ (nominally $^{\rm 5}P_2$) state, whereupon its configuration becomes a mixture of $2p_{1/2}^22p_{3/2}3p_{1/2}$ and $2p_{1/2}2p_{3/2}^23p_{1/2}$. The presence of the $3p_{1/2}$ orbital causes $2^{\rm e}(2)$ to stabilize relative to the ground state, albeit not strongly enough to drive it below $2^{\rm e}(1)$ before c reaches c^{\star} .

The last even-parity state in our current discussion of the oxygen atom is $0^e(2)$, which is labeled 1S_0 at $c=c_0$. For $c_0/10 \le c \le c_0$, the state $0^e(2)$ comprises of the configurations $2p_{1/2}^22p_{3/2}^2$ and $2p_{3/2}^4$, with the latter causing the $0^e(2)$ energy to rise relative to that of the ground state. At $c \approx c_0/10$, however, there occurs an avoided crossing between $0^e(2)$ and the higher lying $0^e(3)$ state (not included in the study), whereupon the dominant configuration in $0^e(2)$ changes to $2p_{1/2}^22p_{3/2}3p_{3/2}$. As c decreases further, this configuration becomes more and more dominant in $0^e(2)$, thus stabilizing this state relative to the ground state, which, to

reiterate, comprises mainly of $2p_{1/2}^2 2p_{3/2}^2$. At even smaller c, more specifically, at $c \approx c_0/12$, $0^e(2)$ becomes involved in another avoided crossing with the same $0^e(3)$. After this second avoided crossing, the dominant configuration in $0^e(2)$ is now $2p_{1/2}^2 3s_{1/2}^2$, which causes its energy to fall even more precipitously. The state $0^e(2)$ does eventually fall below the nominal ground state but this happens very close to the critical c^* .

Finally, we discuss the two odd-parity states, 2° and 1° , which, at $c=c_0$, are labeled $^5S_2^{\circ}$ and $^3S_2^{\circ}$, respectively. The evolutionary patterns of these two states as c varies are qualitatively the same, as evident in the congruence of their corresponding curves. They start out as combinations of $2p_{1/2}^22p_{3/2}3s_{1/2}$, $2p_{1/2}2p_{3/2}^23s_{1/2}$, and $2p_{3/2}^33s_{1/2}$. For $c_0/6 \lesssim c \leq c_0$, the competing lowering of the $3s_{1/2}$ energy and raising of the $2p_{3/2}$ energy results in a slight stabilization of 2° and 1° relative to the ground state. However, for $c \leq c_0/6$, the two configurations with $2p_{3/2}$ doubly and triply occupied drop off from the CI expansions of 2° and 1° , leaving only $2p_{1/2}^22p_{3/2}3s_{1/2}$ which hastens their stabilization. In fact, the state 2° is the first to come below the nominal ground state $2^{\circ}(1)$, at $c \approx c_0/16.5$, thus acting as a 'new' ground state in the interval $c_0/17 \lesssim c \lesssim c_0/16.5$, after which the role of ground state is taken over by $0^{\circ}(1)$. Although the state 1° does cross the nominal ground state, at $c \approx c_0/17$, its higher energy at $c \approx c^*$ means that it never becomes a ground state of oxygen, unlike 2° .

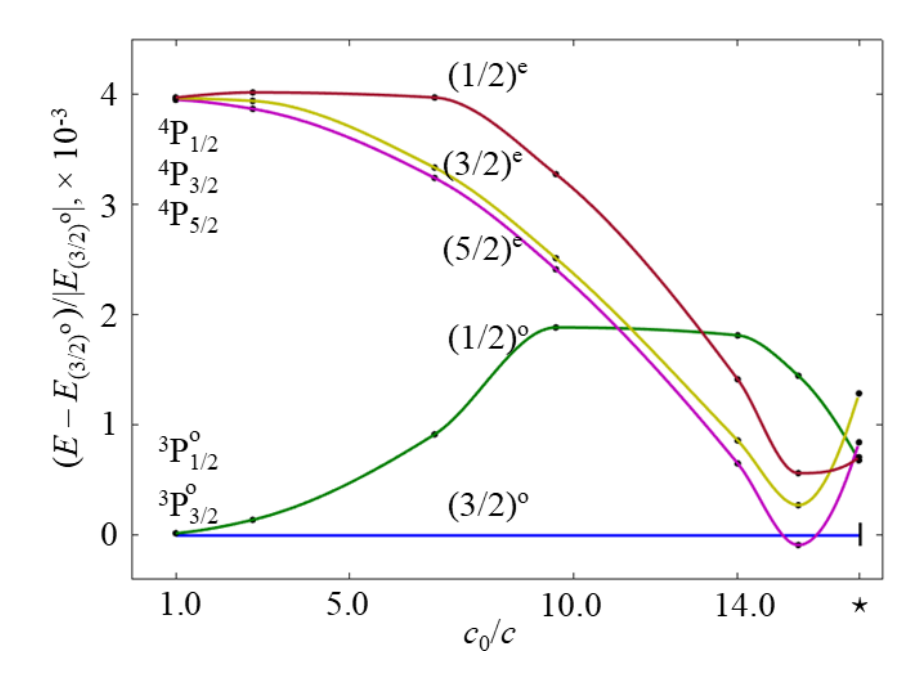


Figure S6. Energy spectrum of a fluorine atom as a function of speed of light (or α). The critical value of c_0/c is marked with star (\star).

In this subsection, we investigate the behavior of atomic fluorine with varying c, limiting ourselves to the five lowest states, see Figure S6. At the nominal c, the $2p^5$ ground electron configuration produces two atomic states with odd parities, $P_{3/2}^o$ and $^2P_{1/2}^o$. From the $2p^43s$ first excited configuration of fluorine we consider three low lying states, which are labeled $^4P_{5/2}$, $^4P_{3/2}$ and $^4P_{1/2}$ at $c=c_0$.

Again, the nominal ground state, labeled $(3/2)^{\rm o}$ for $c < c_0$, is used as a reference. It consists of a single dominant configuration $2p_{1/2}^22p_{3/2}^3$ from $c=c_0$ all the way down to $c\approx c_0/14$ where next possible configuration, $2p_{1/2}^22p_{3/2}3s_{1/2}^2$ as required by the conservation of total angular momentum and parity, emerges as another dominant configuration. This fact may be understood by noting that $2p_{1/2}^22p_{3/2}3s_{1/2}^2$ involves transferring a pair of $2p_{3/2}$ electrons to the higher $3s_{1/2}$ shell and is thus only possible if the $3s_{1/2}$ and $2p_{3/2}$ energies are close enough to each other.

We now discuss the odd-parity excited states. In the region $c_0/10 \lesssim c < c_0$, the state $(1/2)^{\rm o}$ (nominally $^2{\rm P}^{\rm o}_{1/2}$) consists primarily of $2p_{1/2}2p_{3/2}^4$, so its energy rises relative to that of the ground state $(3/2)^{\rm o}$. At $c \lesssim c_0/14$, however, the $2p_{3/2}$ and $3p_{3/2}$ energies come close enough to one another so that the migration of a $2p_{3/2}$ electron to the $3p_{3/2}$ shell happens, accompanied by the filling of the $2p_{1/2}$ shell with another $2p_{3/2}$ electron. As a result, $(1/2)^{\rm o}$ acquires the component $2p_{1/2}^22p_{3/2}^23p_{3/2}$, which causes its energy to slightly lower relative to the ground state energy. When c is reduced beyond $c_0/14$, the energy gaps between $2p_{3/2}$ and $3s_{1/2}$ and between $3p_{1/2}$ and $3p_{3/2}$ become such that its is possible to promote the two $2p_{3/2}$

electrons to $3s_{1/2}$ while demoting at the same time the $3p_{3/2}$ electron to $3p_{1/2}$. As a result, for $c \le c_0/14$, the state $(1/2)^{\circ}$ contains the configuration $2p_{1/2}^2 3s_{1/2}^2 3p_{1/2}$. The stabilizing $3s_{1/2}$ and $3p_{1/2}$ orbitals cause a rapid decline in $(1/2)^{\circ}$ as c approaches c^* .

We now describe the even-parity states. The behaviors of $(5/2)^e$ and $(3/2)^e$ (nominally $^4P_{5/2}$ and $^4P_{3/2}$, respectively) as c varies are very similar. They both start out as combinations of $2p_{1/2}^22p_{3/2}^23s_{1/2}$ and $2p_{1/2}2p_{3/2}^33s_{1/2}$. The configuration $2p_{1/2}^22p_{3/2}^23s_{1/2}$ is responsible for the stabilization of these two states relative to $(3/2)^o$. This stabilization is gradual at first but accelerates after $c \approx c_0/2$, when the energetically unfavorable component $2p_{1/2}2p_{3/2}^3s_{1/2}$ drops off from the CI expansion of $(5/2)^e$ and $(3/2)^e$. As c is reduced further to $c \approx c_0/14$, the configuration $2p_{1/2}^22p_{3/2}3s_{1/2}^2$ appears in the expansion of the ground state and, since the $3s_{1/2}$ energy is still a little higher than that of $2p_{3/2}$, causes the states $(5/2)^e$ and $(3/2)^e$ to stabilize even faster. In fact, $(5/2)^e$ briefly replaces $(3/2)^o$ as the 'new' ground state of fluorine. At $c \approx c_0/15$, however, the $3s_{1/2}$ energy falls below that of $2p_{3/2}$ and this explains the upturn at the rightmost ends of the $(5/2)^e$ and $(3/2)^e$ energy curves.

Finally, we discuss the state $(1/2)^e$ which is labeled $^4P_{1/2}$ at $c=c_0$. For $c_0/6 \lesssim c \leq c_0$, its CI expansion contains the configurations $2p_{1/2}^22p_{3/2}^23s_{1/2}$, $2p_{1/2}2p_{3/2}^33s_{1/2}$, and $2p_{3/2}^43s_{1/2}$. The stabilization of $2p_{1/2}$ and $3s_{1/2}$ competes with the destabilization of $2p_{3/2}$, resulting in a flat pattern of the $(1/2)^e$ energy relative to the ground state energy. For c below $c_0/6$, however, the two configurations with $2p_{3/2}$ triply and quadruply occupied become so energetically unfavorable that they no longer contribute to $(1/2)^e$. The remaining configuration $2p_{1/2}^22p_{3/2}^23s_{1/2}$ leads to a rapid downturn of the $(1/2)^e$ energy. The rise of the $(1/2)^e$ energy relative to the ground state for $c \leq c_0/16$ may again be explained by the crossing of the $2p_{3/2}$ and $3s_{1/2}$ orbitals.

Neon ($c^* \approx c_0/14.8$)

The last atom in our consideration is neon. At the nominal $c = c_0$, the closed-shell $2p^6$ ground electron configuration of neon results in a single atomic state with even parity, 1S_0 . The $2p^53s$ first excited configuration gives rise to four excited states with odd parity: ${}^2[3/2]_2^0$, ${}^2[3/2]_1^0$, ${}^2[1/2]_0^0$, and ${}^2[1/2]_1^0$. The second excited configuration, $2p^53p$, generates a manifold of atomic states with even parity, among which we consider the three lowest states, ${}^2[1/2]_1$, ${}^2[5/2]_3$, and ${}^2[5/2]_2$. We therefore include a total of eight atomic states of neon in our discussion, see Figure 3 in the main text. At smaller c, these states are labeled, in the order they are introduced above, as 0^e , 2^o , $1^o(1)$, 0^o , $1^o(2)$, 1^e , 3^e , and 2^e , respectively.

Again, we use the nominal ground state 0^e , corresponding to 1S_0 at nominal c, as a reference. In the range $c_0/13 \lesssim c \leq c_0$, the 0^e state retains its closed-shell configuration of $2p_{1/2}^22p_{3/2}^4$. At $c \approx c_0/13$, the $3s_{1/2}$ and $2p_{3/2}$ energies become close enough so that $2p_{1/2}^22p_{3/2}^23s_{1/2}^2$ emerges as an appreciable contribution in the CI expansion of 0^e . Note that two electrons are transferred from $2p_{3/2}$ to $3s_{1/2}$ to preserve total angular momentum and parity. The appearance of the open-shell configuration $2p_{1/2}^22p_{3/2}^23s_{1/2}^2$ in the CI expansion of the nominal ground state indicates that at $c \lesssim c_0/16$, neon is no longer chemically inert.

The fact that lowering c has the effect of 'activating' the naturally inert neon may also be understood by considering the state 2° , which corresponds to $^{2}[3/2]_{2}^{\circ}$ at $c=c_{0}$. The main configuration for 2° in the regime $c_{0}/13 \lesssim c \leq c_{0}$ is $2p_{1/2}^{2}2p_{3/2}^{3}3s_{1/2}$ containing the orbital $3s_{1/2}$ which has the effect of destabilizing 2° . As discussed in the previous paragraph, in the vicinity of $c \approx c_{0}/13$, the ground state 0^{e} acquires the component $2p_{1/2}^{2}2p_{3/2}^{2}3s_{1/2}^{2}$. Since the $3s_{1/2}$ orbital still lies above $2p_{3/2}$ in this regime, the 2° energy falls below that of 0^{e} and 2° briefly becomes the 'new' ground state of neon. However, as c nears $c_{0}/14$, the $2p_{3/2}$ and $3s_{1/2}$ orbitals cross, raising 2° back above 0^{e} .

The state $1^{\circ}(1)$ (nominally ${}^{2}[3/2]_{1}^{\circ}$) displays a dependence on varying c similar to that of 2° . In the regime $c_{0}/13 \lesssim c \leq c_{0}$, its CI expansion is dominated by $2p_{1/2}^{2}2p_{3/2}^{3}3s_{1/2}$ and $2p_{1/2}2p_{3/2}^{4}3s_{1/2}$ which stabilize its energy relative to the ground state. However, due to the second configuration where $2p_{3/2}$ is quadruply occupied, the energy of $1^{\circ}(1)$ does not lower as dramatically as that of 2° . In particular, the $1^{\circ}(1)$ energy never falls below the ground state energy. As c approaches then passes $c_{0}/14$, $3s_{1/2}$ crosses below $2p_{3/2}$ and $1^{\circ}(1)$ destabilizes relative to 0° . The rate of destabilization is reduced as c approach c^{\star} due to the appearance of the configuration $2p_{1/2}^{2}2p_{3/2}3s_{1/2}^{2}4s_{1/2}$ in the expansion of $1^{\circ}(1)$.

The last odd-parity state included in our discussion is 0° (nominally $^{2}[1/2]_{0}^{\circ}$) which, for $c_{0}/10 \lesssim c \leq c_{0}$ comprises mainly of $2p_{1/2}2p_{3/2}^{4}3s_{1/2}$ which, similarly to the case of $1^{\circ}(2)$, causes 0° to destabilize relative to the nominal ground state. The energy of 0° rises until $c \approx c_{0}/10$, where an avoided crossing with a higher state of the same total angular momentum and parity (not included in this study) changes the configuration of 0° to $2p_{1/2}^{2}2p_{3/2}^{3}3d_{5/2}$. Since the $3d_{5/2}$ orbital destabilizes with decreasing c at a much slower rate than $2p_{3/2}$, the 0° energy experiences a steep downturn relative to the ground state energy for $c \lesssim c_{0}/10$.

Next, we consider the even-parity excited states 1^e and 2^e , which correspond to ${}^2[1/2]_1$ and ${}^2[5/2]_2$ at $c=c_0$. These states both start out at as combinations of $2p_{1/2}^22p_{3/2}^33p_{1/2}$ and $2p_{1/2}^22p_{3/2}^33p_{3/2}$. As c is reduced, the $3p_{1/2}$ energy decreases and the $3p_{3/2}$ energy increases at a much slower rate than that of $2p_{1/2}$. As a result, the states 1^e and 2^e generally destabilize with respect to the nominal ground state 0^e . However, the stabilization pattern of 2^e displays a peculiar feature. At $c \approx c_0/13$, the configuration $2p_{1/2}^22p_{3/2}^33p_{3/2}$ is replaced by $2p_{1/2}^22p_{3/2}^23s_{1/2}^2$ from the CI expansion of 1^e and 2^e . As a result, the decrease of the 2^e energy becomes even more precipitous and at $c \approx c_0/14$, it becomes less than the 0^e energy, thus making 2^e the new ground state of neon.

Finally, we consider the state 3^e , which is labeled ${}^2[5/2]_3$ at $c=c_0$. The dominant configuration in state remains $2p_{1/2}^22p_{3/2}^33p_{3/2}$ for all $c^* \leq c \leq c_0$. As a result, it destabilizes continuously relative to the ground state, albeit not rapidly enough for it to cross the nominal ground state anywhere in the interval $c^* \leq c \leq c_0$.

Section IV. Effect of varying speed of light on electronic structure of water and ammonia

In relativistic picture, the states of atoms and molecules are described by four component Dirac spinors $\psi = (\psi_L^{\alpha}, \psi_L^{\beta}, \psi_S^{\alpha}, \psi_S^{\beta})^T$, where L and S correspond to the large and small components of the spinor (not to be confused with the total orbital angular and spin momenta), and α and β describe spin degrees of freedom. The spinor components are in general complex numbers, so a general collection of four such components has eight degrees of freedom. However, since the spatial and spin degrees of freedom are coupled, the symmetry of the Dirac spinors is described by the double groups, where the total spinor transforms under the fermion irreducible representations spanned by the half-integer spin functions. Furthermore, the real and imaginary parts of each spinor component are spanned by boson irreducible representations, which are the irreducible representations of conventional single point groups. Therefore, each spinor component can be described by scalar functions, or orbitals.

The symmetries of the ammonia and water molecules are described by the C_{3v} and C_{2v} double groups. For example, exploiting the symmetry of the Dirac Hamiltonian, it can be shown that in the C_{2v} double group, the real and imaginary parts of the large component transform under (a_1, a_2) and (b_1, b_2) boson irreducible representations for ψ_L^{α} and ψ_L^{β} , correspondingly. At nominal c, molecular orbitals of ammonia and water are spanned only by a real or imaginary part of a single component, neglecting the vanishing contributions from other components. Therefore, these orbitals are described by a single irreducible representation, in compliance with results from non-relativistic calculations. At decreased c, however, the molecular orbitals are spanned by multiple real and imaginary parts of the spinor components. Therefore, no longer a single irreducible representation can be assigned to molecular orbitals. For this reason, the symmetry labels in MO diagrams of ammonia and water are presented only at nominal speed of light, but not for smaller c.

In the MO diagram for water (Figure 3a-c in the main text), the σ and σ^* linear combinations of 1s orbitals of two hydrogen atoms have the a_1 and b_2 symmetries. For oxygen at nominal c, the atomic orbitals $2s_{1/2}$ and $3s_{1/2}$ have the symmetry of a_1 whereas the 2p orbitals have the symmetries a_1 , b_1 , and b_2 . In the ammonia MO diagram (Figure 3d-f), the three linear combinations ψ_1 , ψ_2 , and ψ_3 of 1s orbitals belonging to three hydrogen atoms have a_1 and doubly degenerate e symmetries. At nominal c, the $2s_{1/2}$ and $3s_{1/2}$ atomic orbitals of nitrogen have symmetry a_1 , whereas the 2p orbitals have symmetries a_1 and e. In atomic calculations of oxygen and nitrogen, the $3s_{1/2}$ spinor was included in the average-of-configuration Dirac-Hartree-Fock method to assess effect of stabilization of higher lying spinors on molecular bonding. For clearer comparison of diagrams, we keep the energy unit constant and equal to those at nominal c. To better demonstrate the changes in the electronic structure of molecules at the decreased speeds of light, we calculated the radial density distribution in DIRAC19^{8,9} for each molecular orbital of water and ammonia as

$$\rho(r) = \int_{0}^{2\pi} d\theta \sin\theta \int_{0}^{\pi} d\varphi \, \rho(\mathbf{r}) r^{2}, \qquad (23)$$

where $\rho(r) \equiv |\Psi(r)|^2$ is the electron density and $\Psi(r)$ is the MO wavefunction.

Water

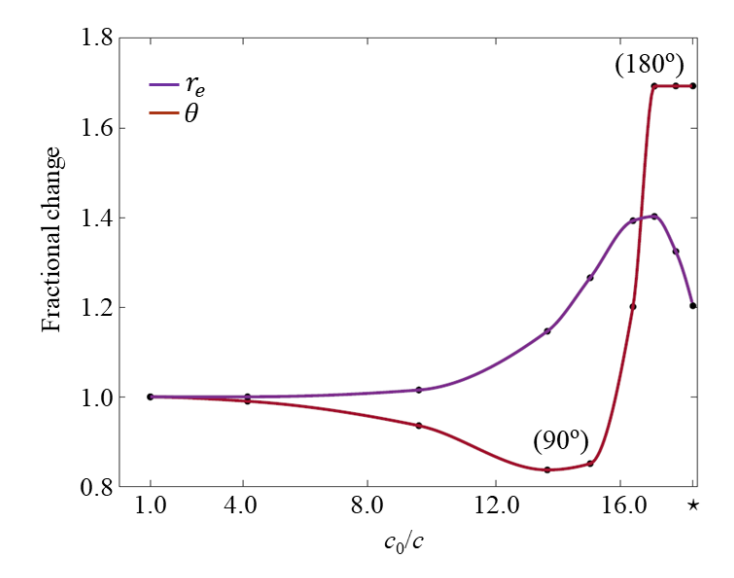


Figure S7. Changes in equilibrium geometry of a water molecule induced by variation of c from nominal to critical value (marked with \star on the x-axis): $c_0^{\star} = 7.46$ (or equivalently $c_0/c_0^{\star} = 18.4$). The changes in the O-H bond distance and the H-O-H bond angle are shown as fractional changes.

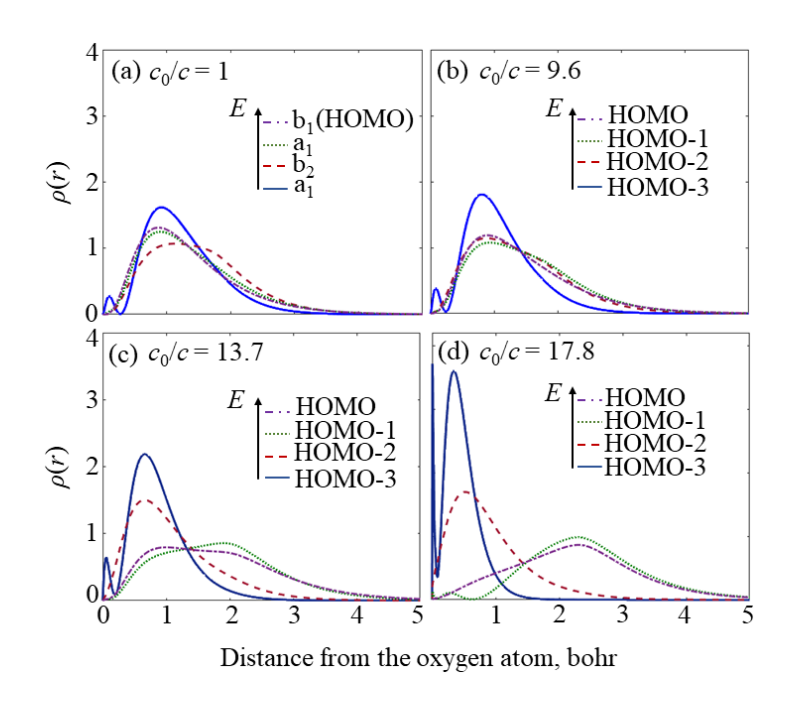


Figure S8. Radial density distributions (RDDs) of four MOs of water at different values of *c*. The oxygen atom is put to the coordinate origin. The MOs are given in the increasing energy order: dark blue solid line (HOMO-3), dark red dashed line (HOMO-2), dark green dotted line (HOMO-1), and magenta dot-dashed line (HOMO). For clearer comparison, distance is given in unit of unscaled nominal bohr radius.

Ammonia

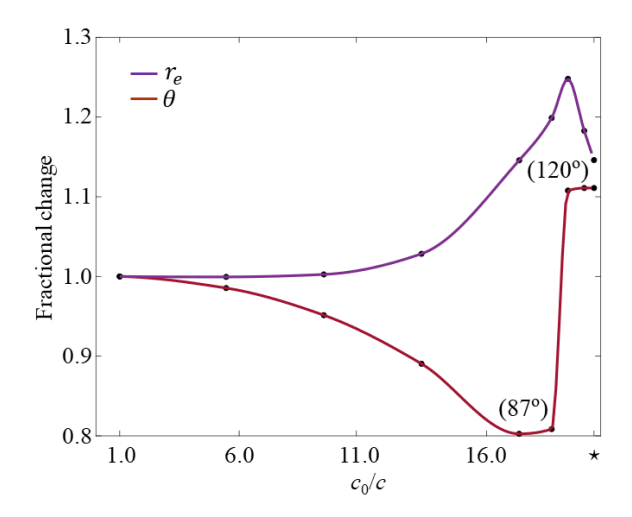


Figure S9. Changes in equilibrium geometry of an ammonia molecule induced by variation of c from nominal to critical value (marked with \star on the x-axis): $c_N^{\star} = 6.5$ (or equivalently $c_0/c_N^{\star} = 20.9$). The changes in the N-H bond distance and the H-N-H bond angle are shown as fractional changes.

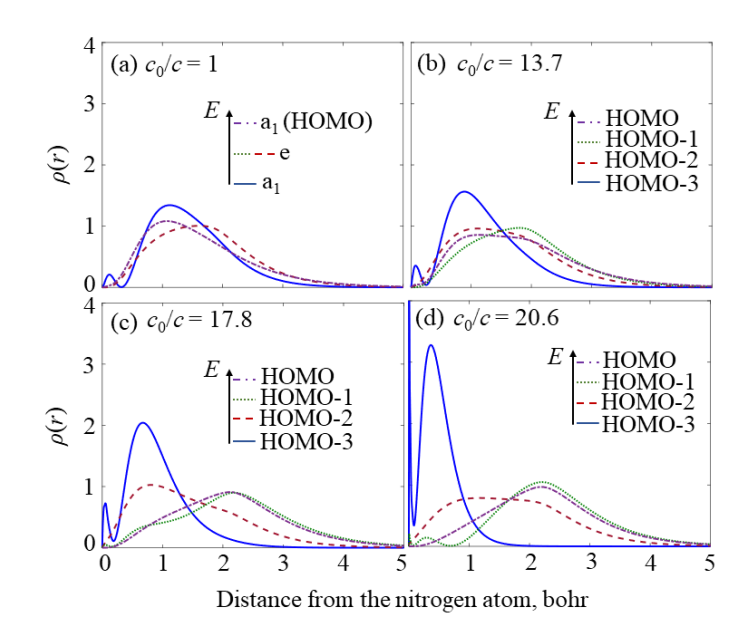


Figure S10. Radial density distributions (RDDs) of four valence MOs of ammonia at different values of the speed of light *c*. The nitrogen atom is put to the coordinate origin. The MOs are given in the increasing energy order: dark blue solid line (HOMO-3), dark red dashed line (HOMO-2), dark green dotted line (HOMO-1), and magenta dot-dashed line (HOMO). For clearer comparison, distance is given in unit of unscaled nominal bohr radius.

Section V. Dipole moments of water and ammonia at the nominal, intermediate, and near critical values of the speed of light

The dipole moments of water and ammonia were calculated at the selected four-component Dirac-Hartree-Fock optimized geometries – W_1 ($c = c_0$, $r_{OH} = 0.939$ Å, $\theta = 106.3^{\circ}$), W_2 ($c \approx$ $c_0/13.7$, $r_{\rm OH} = 1.077$ Å, $\theta = 89.0^{\circ}$), and $\mathbf{W_3}$ ($c \approx c_0/17.8$, $r_{\rm OH} = 1.244$ Å, $\theta = 180.0^{\circ}$) – for water, and A_1 ($c = c_0$, $r_{NH} = 0.997$ Å, $\theta = 108.1^\circ$, dihedral angle = 116.8°), A_2 ($c \approx c_0/17.8$, $r_{\rm NH} = 1.143 \text{ Å}, \ \theta = 87.0^{\circ}, \ \text{dihedral angle} = 88.1^{\circ}, \ \text{and} \ \mathbf{A_3} \ (c \approx c_0/20.6, \ r_{\rm NH} = 1.180 \ \text{Å}, \ \theta = 1.180 \ \text{Å}$ 120.1° , dihedral angle = 179.8°) – for ammonia. The values of the bond distances are given unscaled for varying c. The change in the dipole moment at varying c comes predominantly from the change in the molecular geometry induced by increased relativistic effects, and the relativistic correction to the electronic structure is considered to be minor. Therefore, the dipole moments were calculated in the non-relativistic approximation with, however, included scalar relativistic effects. The calculations were performed in MOLPRO. 13 The dipole moments were calculated using the internally contracted multireference configuration interaction (IC-MRCI) method with the single and double excitations with the aug-cc-pCV6Z basis set. The reference complete active space self-consistent field (CASSCF) wavefunctions for the MRCI step were obtained by including four electrons and eight orbitals in the active space: CASSCF(4,8). The electrons of the core 1a1 MO of water (ammonia) were not included in the active space but were correlated as well in the MRCI calculations (no frozen core).

At nominal c, our calculated dipole moment of 1.872 D compares well with the measured value of 1.855 D. At the 14-fold reduction of c ($c \approx c_0/13.7$) the bond angle in water contracts from 106.3° (104.5°) to 89.0°. This should result in an increased dipole moment; indeed, our calculations for W_2 predict the dipole moment of 2.138 D. At near critical c, the water becomes linear and therefore the dipole moment becomes zero. Similar changes are observed for the dipole moment of ammonia. This is due to similar relative changes in energies of the $2p_{1/2}$, $2p_{3/2}$, and $3s_{1/2}$ atomic orbitals of nitrogen and oxygen at reduced speed of light. For A_1 , our calculated dipole moment of 1.482 D is slightly different from the measured value of 1.561 D. This discrepancy can be explained by the deviation of $r_{\rm NH} = 0.997$ Å and $\theta = 108.1^{\circ}$ of A_1 from the accepted $r_{\rm NH} = 1.012$ Å and $\theta = 106.7^{\circ}$. Indeed, the dipole moment of 1.526 D calculated with the accepted values $r_{\rm NH}$ and θ is much closer to the measured moment. At the smallest value of $\theta = 87.0^{\circ}$ ($c \approx c_0/17.8$), the dipole moment is increased to 2.028 D. At $c \approx c_0/20.6$, ammonia becomes trigonal planar with the zero net dipole moment.

References

- (1) Greiner, W.; Reinhardt, J. Quantum Electrodynamics; Springer Berlin Heidelberg, 2008.
- (2) Zeldovich, Y.B.; Popov, V.S. Electronic Structure of Superheavy Atoms. *Sov. Phys. Uspekhi* **1972**, *14*, 673-694.
- (3) Tiesinga, E.; Mohr, P. J.; Newell, D. B.; Taylor, B. N. The 2018 CODATA Recommended Values of the Fundamental Physical Constants. Tech. Rep. National Institute of Standards and Technology. https://physics.nist.gov/cuu/Constants/index.html (accessed 2024-03-18).
- (4) Johnson, W. *Atomic Structure Theory: Lectures on Atomic Physics*; Springer-Verlag Berlin Heidelberg, 2007.
- (5) Johnson, W.; Soff, G. The Lamb Shift in Hydrogen-Like Atoms, $1 \le Z \le 110$. *At. Data Nucl. Data Tables* **1985**, *33*, 405-446.
- (6) Ferreira, E. M.; Sesma, J. Zeros of the Macdonald Function of Complex Order. *J. Comput. Appl. Math.* **2008**, *211*, 223-231.
- (7) Saue, T.; Jensen, H. J. A. Quaternion Symmetry in Relativistic Molecular Calculations: The Dirac-Hartree-Fock Method. *J. Chem. Phys.* **1999**, *111*, 6211-6222.
- (8) Saue, T.; Bast, R.; Gomes, A. S. P.; Jensen, H. J. A.; Visscher, L.; Aucar, I. A.; Di Remigio, R.; Dyall, K. G.; Eliav, E.; Fasshauer, E.; et al. The DIRAC Code for Relativistic Molecular Calculations. *J. Chem. Phys.* **2020**, *152*, 204104.
- (9) Brown, G. E.; Ravenhall, D. G.; Peierls, R. E. On the Interaction of Two electrons. *Proc. R. Soc. Lond.* **1951**, *208*, 552-559.
- (10) Sapirstein, J. Theoretical Methods for the Relativistic Atomic Many-Body Problem. *Rev. Mod. Phys.* **1998**, *70*, 55-76.
- (11) Barysz, M.; Ishikawa, Y. Relativistic Methods for Chemists; Springer, Dordrecht, 2010.
- (12) Dzuba, V. A.; Flambaum, V. V.; Webb, J. K. Calculations of the Relativistic Effects in Many-Electron Atoms and Space-Time Variation of Fundamental Constants. *Phys. Rev.* A **1999**, *59*, 230-237.
- (13) Werner, H.-J.; Knowles, P. J.; Knizia, G.; Manby, F. R.; Schütz, M. Molpro: A General-Purpose Quantum Chemistry Program Package. *Wiley Interdiscip. Rev. Comput. Mol. Sci.* **2012**, *2*, 242–253.
- (14) Lodi, L.; Tolchenov, R. N.; Tennyson, J.; Lynas-Gray, A. E.; Shirin, S. V.; Zobov, N. F.; Polyansky, O. L.; Császár, A. G.; Van Stralen, J. N. P.; Visscher, L. A New Ab Initio Ground-State Dipole Moment Surface for the Water Molecule. *J. Chem. Phys.* **2008**, *128*, 044304.
- (15) Yurchenko, S. N.; Carvajal, M.; Lin, H.; Zheng, J.; Thiel, W.; Jensen, P. Dipole Moment and Rovibrational Intensities in the Electronic Ground State of NH₃: Bridging the Gap between Ab Initio Theory and Spectroscopic Experiment. *J. Chem. Phys.* **2005**, *122*, 104317.